
Doctoral Dissertations

Student Theses and Dissertations

Fall 2020

Tools to evaluate nanodiamond-mediated delivery of tiopronin for cataract prevention

Justin Beltz

Follow this and additional works at: https://scholarsmine.mst.edu/doctoral_dissertations

 Part of the [Analytical Chemistry Commons](#), and the [Biochemistry Commons](#)

Department: Chemistry

Recommended Citation

Beltz, Justin, "Tools to evaluate nanodiamond-mediated delivery of tiopronin for cataract prevention" (2020). *Doctoral Dissertations*. 2946.

https://scholarsmine.mst.edu/doctoral_dissertations/2946

This thesis is brought to you by Scholars' Mine, a service of the Missouri S&T Library and Learning Resources. This work is protected by U. S. Copyright Law. Unauthorized use including reproduction for redistribution requires the permission of the copyright holder. For more information, please contact scholarsmine@mst.edu.

TOOLS TO EVALUATE NANODIAMOND-MEDIATED DELIVERY OF
TIOPRONIN FOR CATARACT PREVENTION

by

JUSTIN EDWARD BELTZ

A DISSERTATION

Presented to the Graduate Faculty of the
MISSOURI UNIVERSITY OF SCIENCE AND TECHNOLOGY

In Partial Fulfillment of the Requirements for the Degree

DOCTOR OF PHILOSOPHY

in

CHEMISTRY

2020

Approved by:

Nuran Ercal, Advisor
Klaus Woelk
Chariklia Sotiriou-Leventis
Honglan Shi
Yue-Wern Huang

© 2020

Justin Edward Beltz

All Rights Reserved

PUBLICATION DISSERTATION OPTION

This dissertation consists of the following three articles, formatted in the style used by the Missouri University of Science and Technology:

Paper I, found on pages 7–34, has been published in *Free Radical Research* 2020;54(5):319-329.

Paper II, found on pages 35–58, has been published in *Biomedical Chromatography* 2018;e4375.

Paper III, found on pages 59–88, has been published in *Diamond and Related Materials* 2019;107590.

ABSTRACT

There is a growing demand for non-surgical means of cataract treatment. This dissertation presents three bodies of work that reflect the early-stage development of eye drop formulations aimed at delaying cataract progression. These formulations consist of the antioxidant 2-mercaptopropionylglycine (MPG) loaded onto nanodiamond particles.

Cataractogenesis is linked to oxidative damage to lens proteins. To investigate the potential of MPG for protection against oxidative damage, A549 cells were incubated in 0.6 mM *tert*-butylhydroperoxide (*t*BHP). Cells exposed to *t*BHP without MPG exhibited elevated levels of reactive oxygen species, which led to the depletion of the vital antioxidant glutathione and, ultimately, apoptosis. Co-administration of 5 mM MPG protected cells from *t*BHP-induced damage, resulting in maintenance of cell viability.

To monitor the uptake and fate of MPG in the eye, a rapid, high sensitivity HPLC method was developed for the analysis of MPG and its metabolite, 2-mercaptopropionic acid, in ocular tissues. Method validation experiments demonstrated the reliability of this method for quantifying MPG uptake and evaluating drug delivery strategies.

Achieving effective drug concentrations in the lens poses a major challenge. Nanodiamond is biocompatible, and its surface chemistry can be tailored to specific applications. Thus, it is emerging as a candidate of interest for drug delivery. Nanodiamond surfaces were functionalized with carboxyl (ND-COOH), hydroxyl (ND-OH), and amino (ND-NH₂) groups to investigate the effect of ND surface chemistry on adsorption and release of MPG. The ND-NH₂ exhibited the highest adsorption capacity, but the ND-OH was the most effective for sustained release.

ACKNOWLEDGMENTS

Firstly, I would like to thank my advisor, Dr. Nuran Ercal, for her continued support and guidance throughout my residence at Missouri S&T. She has provided me with countless opportunities for growth and development as a scientist.

I would also like to thank Dr. Vadym Mochalin and the members of my committee, Drs. Klaus Woelk, Lia Leventis, Honglan Shi, and Yue-Wern Huang.

I am thankful for the mentorship and camaraderie provided by my former and current research group members, especially Annalise Pfaff, Hsiu-Jen Wang, Yasaswi Maddirala, Anna Chernatynskaya, and Ibrahim Abdullahi.

I must also acknowledge the late Richard K. Vitek, whose financial contributions supported the research activities and scientific development of myself as well as countless other students.

Finally, I would like to thank my friends and family for encouraging me through this journey, especially my parents, who supported my lifelong dream of becoming a scientist.

TABLE OF CONTENTS

	Page
PUBLICATION DISSERTATION OPTION	iii
ABSTRACT	iv
ACKNOWLEDGMENTS	v
LIST OF ILLUSTRATIONS	xi
LIST OF TABLES	xiii
NOMENCLATURE	xiv
 SECTION	
1. INTRODUCTION	1
1.1. GLOBAL HEALTH IMPACT OF CATARACTS	1
1.2. CATARACTOGENESIS AND AVENUES FOR TREATMENT	1
1.2.1. Tiopronin	3
1.2.2. Eye Drops Are the Preferred Route of Administration	4
1.2.3. Drug Delivery Vehicles Can Promote MPG Uptake and Efficacy.	4
1.2.4. Nanodiamond Drug Delivery	4
1.3. DEVELOPMENT AND EVALUATION OF ND:MPG FORMULATIONS ...	6
 PAPER	
I. PROTECTIVE EFFECTS OF TIOPRONIN ON OXIDATIVELY CHALLENGED HUMAN LUNG CARCINOMA EPITHELIAL CELLS (A549) ..	7
ABSTRACT	7
1. INTRODUCTION	8
2. MATERIALS AND METHODS	10

2.1. CHEMICALS AND REAGENTS.....	10
2.2. CELL CULTURE AND PRELIMINARY EXPERIMENTS	11
2.3. EXPERIMENTAL DESIGN	12
2.4. CELL VIABILITY	13
2.5. QUANTIFICATION OF INTRACELLULAR GSH LEVEL.....	13
2.6. FLOW CYTOMETRY ANALYSIS OF APOPTOTIC CELLS AND INTRACELLULAR ROS MEASUREMENT.....	15
2.7. FLOW CYTOMETRY DETERMINATION OF MITOCHONDRIAL SUPEROXIDE	16
2.8. STATISTICAL ANALYSIS	17
3. RESULTS AND DISCUSSION	17
3.1. SELECTION OF DOSING CONCENTRATIONS	17
3.2. EFFECT OF MPG ON INTRACELLULAR GSH IN OXIDATIVELY CHALLENGED A549 CELLS	20
3.3. EFFECT OF MPG ON VIABILITY OF OXIDATIVELYCHALLENGED A549 CELLS.....	20
3.4. EFFECT OF TREATMENT ON APOPTOTIC AND NECROTIC CELL POPULATIONS.....	22
3.5. DISTRIBUTION OF CELLS WITH ROS PRESENT IN APOPTOTIC AND NON-APTOPTOTIC SUBPOPULATIONS	24
3.6. DISTRIBUTION OF SUPEROXIDE PRESENT IN MITOCHONDRIA OF APOPTOTIC AND NON-APOPTOTIC POPULATIONS.....	26
4. CONCLUSIONS	28
ACKNOWLEDGMENTS.....	29
FUNDING DETAILS	29
DISCLOSURE STATEMENT.....	30

DATA AVAILABILITY STATEMENT AND DATA DEPOSITION	30
REFERENCES	30
II. SIMULTANEOUS DETERMINATION OF TIOPRONIN AND ITS PRIMARY METABOLITE IN PLASMA AND OCULAR TISSUES BY HPLC	35
ABSTRACT	35
1. INTRODUCTION	36
2. EXPERIMENTAL METHODS	40
2.1. CHEMICALS AND REAGENTS	40
2.2. ANIMALS	41
2.3. SAMPLE PREPARATION	41
2.4. PREPARATION OF CALIBRATION STANDARDS	42
2.5. HPLC PARAMETERS	43
2.6. METHOD VALIDATION	44
2.6.1. Selectivity	44
2.6.2. Linearity and LLOQ	44
2.6.3. Sample Stability	44
2.6.4. Precision, Accuracy, and Recovery	45
3. RESULTS AND DISCUSSION	45
3.1. CHROMATOGRAPHY	46
3.2. SELECTIVITY	49
3.3. LINEARITY AND LLOQ	49
3.4. SAMPLE STABILITY	51
3.5. PRECISION, ACCURACY, AND RECOVERY	53

3.6. DETERMINATION OF MPG AND MPA IN PLASMA AND OCULAR TISSUES	53
4. CONCLUSION	55
ACKNOWLEDGMENTS	56
REFERENCES	56
III. EFFECT OF NANODIAMOND SURFACE CHEMISTRY ON ADSORPTION AND RELEASE OF TIOPRONIN	59
ABSTRACT	59
1. INTRODUCTION	60
2. EXPERIMENTAL METHODS	63
2.1. MATERIALS AND REAGENTS	63
2.2. PURIFICATION AND SURFACE MODIFICATION OF ND	63
2.3. CHARACTERIZATION OF FUNCTIONALIZED ND	65
2.4. ADSORPTION STUDY	66
2.5. RELEASE STUDY	68
3. RESULTS AND DISCUSSION	69
3.1. CHARACTERIZATION OF FUNCTIONALIZED ND	69
3.2. ADSORPTION OF TIOPRONIN	73
3.3. RELEASE STUDY	77
4. CONCLUSION	81
FUNDING	82
AUTHOR CONTRIBUTIONS	82
DECLARATIONS OF INTEREST	83
SUPPORTING INFORMATION	83

REFERENCES.....	86
SECTION	
2. CONCLUSIONS.....	89
2.1. TO WHAT EXTENT DOES MPG PROTECT CELLS AGAINST ACUTE OXIDATIVE INSULT?.....	89
2.2. HOW WILL MPG BE MEASURED IN CELL AND ANIMAL MODELS?.....	90
2.3. WHAT IS THE OPTIMAL ND SURFACE CHEMISTRY FOR ADSORPTION AND RELEASE OF MPG?.....	91
2.4. FUTURE DIRECTIONS.....	92
BIBLIOGRAPHY.....	94
VITA.....	98

LIST OF ILLUSTRATIONS

PAPER I	Page
Figure 1. A. Plot of cell viability vs. <i>t</i> BHP concentration. B. Plot of intracellular GSH concentration vs. <i>t</i> BHP concentration.....	18
Figure 2. Plot of intracellular GSH concentration vs. dosing concentration of MPG.	19
Figure 3. A. Plot of treatment vs. intracellular GSH concentration. B. Plot of treatment vs. cell viability.....	21
Figure 4. Representative dot-plots from flow cytometry analysis of apoptotic cells.	23
Figure 5. Representative dot-plots from flow cytometry analysis of ROS in apoptotic and live subpopulations.....	25
Figure 6. Representative dot-plots of from flow cytometry analysis of superoxide in mitochondria.....	27
PAPER II	
Figure 1. Hydrolysis of MPG to MPA.....	37
Figure 2. Derivatization of thiols with ThioGlo-3.....	40
Figure 3. Overlay of representative chromatograms from samples containing A, ThioGlo-3 in sample diluent; B, ThioGlo-3 + TCEP; C, ThioGlo-3 + TCEP + NAC; D, ThioGlo-3 + TCEP + NAC + MPA; E, ThioGlo-3 + TCEP + NAC + MPG + MPA.....	47
Figure 4. Derivatization of thiols containing a stereocenter gives rise to products with two stereocenters.....	48
Figure 5. Representative chromatograms from processed tissue samples.....	50
Figure 6. Calibration curves for MPG (left) and MPA (right) diluted in SBB.....	51
PAPER III	
Figure 1. Tiopronin microspecies in equilibrium.	61

- Figure 2. A. Low resolution and B. High resolution TEM micrographs of ND-COOH showing 0.206 nm d-spacing. C. Selected area electron diffraction pattern of ND-COOH sample consistent with small ND primary particle size and diffraction rings corresponding to the (111), (220), and (311) planes of diamond. 70
- Figure 3. A. XRD pattern of as-received ND. B. FTIR spectra of as-received ND, ND-COOH, ND-OH, and ND-NH₂. C. FTIR spectra of ND-COOH and ND-NH₂ in the range of wavelength corresponding to Amide bands. D. ζ -potential vs. pH and E. Mean diameter of ND agglomerates vs. pH for ND-COOH (●), ND-OH (■), and ND-NH₂ (▲). 71
- Figure 4. A-C. Langmuir (solid red line) and Freundlich (blue dashed line) fits to experimental adsorption isotherms of A. ND-COOH, B. ND-OH, and C. ND-NH₂. D. Overlay of Langmuir fits from A-C. 74
- Figure 5. A. K_L vs. A_{max} B. Separation factor R_L vs. C_0 76
- Figure 6. A-C. Plots of cumulative tiopronin release as a percentage of the initial amount of adsorbed tiopronin vs. time for A. ND-COOH, B. ND-OH, and C. ND-NH₂ in pH 4.0 (●), 5.8 (■), 7.3 (▲), and 8.1 (▼) buffer. D-E. Cumulative tiopronin release after 1 day and 12 days, expressed as D. percentage of the initial amount of adsorbed tiopronin and E. mass of tiopronin released per gram of ND. 78

LIST OF TABLES

PAPER I	Page
Table 1. Treatment media compositions.....	13
Table 2. Effects of exposure to <i>t</i> BHP and treatment with MPG on viable, apoptotic, and necrotic subpopulations.	23
Table 3. Effects of <i>t</i> BHP exposure and MPG treatment on percentage of ROS+ cells in apoptotic and live cell populations.....	26
Table 4. Effects of exposure to <i>t</i> BHP and MPG on the percentage of MSR+ cells in apoptotic and live cell populations.....	28
PAPER II	
Table 1. Detector settings	43
Table 2. Summary of linear regression	51
Table 3. Stability of derivatized samples.....	52
Table 4. Precision, accuracy, and recovery.....	53
Table 5. MPG and MPA concentration in Wistar rat tissues 40 min after intraperitoneal administration of MPG.....	54
PAPER III	
Table 1. Parameters and Pearson's correlation coefficient for Langmuir and Freundlich curve fits to adsorption data	75
Table 2. Calculated distribution of tiopronin microspecies and ζ -potential of ND suspensions.....	79

NOMENCLATURE

Abbreviation	Description
7-AAD	7-Amino-Actinomycin D
A549	Adenocarcinomic Human Alveolar Basal Epithelial Cell Line
ANOVA	Analysis of Variance
Carboxy-H ₂ DCFDA	6-Carboxy-2',7'-Dichlorofluorescein Diacetate
DETAPAC	Diethylenetriaminepentaacetic Acid
DMF	Dimethylformamide
FBS	Fetal Bovine Serum
FL	Fluorescence
FTIR	Fourier Transform Infrared Spectroscopy
GSH	Glutathione
HPLC	High Performance Liquid Chromatography
MPA	2-Mercaptopropionic Acid; Thiolactic Acid
MPG	2-Mercaptopyrnyl Glycine; Tiopronin
MSR	MitoSOX Red Mitochondrial Superoxide Indicator
MTT	3-(4,5-Dimethylthiazol-2-yl)-2,5-Diphenyltetrazolium Bromide
NAC	N-Acetylcysteine
NACA	N-Acetylcysteine amide
ND	Nanodiamond
ND-COCl	Nanodiamond Acyl Chloride
ND-COOH	Carboxylated Nanodiamond

ND-NH ₂	Aminated Nanodiamond
ND-OH	Hydroxylated Nanodiamond
NPM	N-(1-Pyrenyl)maleimide
<i>R</i>	Pearson's Correlation Coefficient
ROS	Reactive Oxygen Species
SAED	Small-Area Electron Diffraction
SAUD	Salt-Assisted Ultrasonic Deaggregation
SBB	Serine Borate Buffer
SDS	Sodium Dodecyl Sulfate
<i>t</i> BHP	<i>tert</i> -Butylhydroperoxide
TCEP	Tris(2-Carboxyethyl)Phosphine)
TEM	Transmission Electron Microscopy
XRD	X-Ray Diffraction

1. INTRODUCTION

1.1. GLOBAL HEALTH IMPACT OF CATARACTS

Cataracts are characterized by a cloudy opacification of the ocular lens that progressively worsens to the point of complete vision loss. They are also the leading cause of blindness worldwide.¹ Currently, the only available treatment for patients with cataracts is surgical removal of the cataractous lens and subsequent implantation of an artificial lens. Although this procedure is routine and relatively safe, it is not without drawbacks. As with any surgery, there is a risk of serious complications such as capsular rupture, loss of vitreous, and endophthalmitis.² In addition, artificial lenses lack several important properties of natural lenses. The natural lens is able to stretch, allowing for accommodation or focusing on objects or features at a variety of distances. Artificial lenses from cataract surgery do not recapitulate this ability. Furthermore, research conducted by Lim et al. suggests that the natural lens plays a significant role in maintaining ocular health.³ It serves as a reservoir for the vital antioxidant glutathione (GSH), protecting neighboring structures from oxidative damage. With this reservoir removed, patients may be at a greater risk of developing other oxidative stress-related eye disorders such as macular degeneration. Therefore, there is a high demand for non-invasive pharmaceutical alternatives to surgery to treat, prevent, or delay cataract formation.

1.2. CATARACTOGENESIS AND AVENUES FOR TREATMENT

The lens contains highly ordered layers of tightly packed cells known as lens fibers. The refractive power and transparency of the lens is attributed to water-soluble

proteins known as crystallins which compose more than 90% of the protein content of the lens.^{4,5} Oxidative damage can disrupt the native structure of these proteins, resulting in aggregation and loss of transparency. Thus, cataracts are attributed to the aggregation of crystallins. The primary source of oxidative damage in cataracts is most likely ultraviolet radiation; however, other contributing sources of oxidative stress include injury, genetic mutation, and exposure to toxicants or ionizing radiation.

In order to maintain transparency, the nuclear portion of the lens forgoes light-scattering organelles such as nuclei, mitochondria, and endoplasmic reticula.⁶ As a result, lens fiber cells are less metabolically active than most tissues, and once these cells mature, the crystallins are not replaced. Therefore, oxidative damage to crystallin proteins accumulates over a person's lifetime, progressively worsening with age. It is well documented that damage to these proteins is correlated to their aggregation.^{7,8} Oxidation of cysteine and methionine residues progressively increase with cataract severity until >90% of cysteine residues and 50% of methionine residues are oxidized.⁷ Oxidation of cysteine residues in crystallin proteins is noteworthy because it results in intra- and inter-protein cross-linking, altering the native structure of the protein, decreasing the solubility and thus, lens transparency.

Crystallins rely heavily on endogenous antioxidants such as GSH to protect them from oxidative damage in order to preserve their normal structure and function.^{3,8,9} However, levels of these endogenous antioxidants decrease significantly with age,^{10,11} leaving the lens vulnerable to oxidative insult.^{12,13} Indeed, reports have shown that more than 60% of GSH is depleted in cataractous lenses.⁸

Since loss of endogenous antioxidant defenses is so strongly correlated with the progression of age-related nuclear cataract, bolstering these defenses with exogenous antioxidants is one of the primary treatment strategies being explored for delaying cataract progression.

Supplementing GSH directly is impractical due to its low membrane permeability and enzymatic degradation; however, other thiol-containing antioxidants have shown some promise. Thiol antioxidants can scavenge ROS and undergo thiol-disulfide exchange with oxidized cysteine residues. Indeed, reports in the literature demonstrate that thiol antioxidants may prevent or ameliorate cataracts.^{14, 15}

1.2.1. Tiopronin. Tiopronin, formally known as 2-mercaptopropionyl glycine (MPG), is an FDA-approved thiol antioxidant that is used clinically to treat cystinuria. Patients with cystinuria have high levels of cystine in their urine, resulting in cystine kidney stones. Tiopronin undergoes thiol-disulfide exchange with cystine to form tiopronin-cysteine, which is more urine-soluble. This thiol-disulfide exchange, in combination with the capacity for scavenging ROS, may be beneficial for protecting against oxidative insults and reducing crystallin protein disulfides in the lens.

In fact, MPG has demonstrated anticataract effects in various animal and cell models¹⁶⁻²⁰ and even human cataract patients.²¹ Although these results are promising, the routes of administration used are impractical for human patients. When MPG is administered orally, very high doses are required for it to accumulate in the lens. This is attributed to the fact that the lens lacks a direct, dedicated blood supply. Maintaining such high doses can result in several systemic side effects.^{22, 23}

1.2.2. Eye Drops Are the Preferred Route of Administration. Eye drops offer several advantages over oral and other systemic routes of administration. They are easy to administer and allow for localized application to the target organ, circumventing the need for high systemic doses and reducing the risk and severity of side effects. However, this approach poses challenges as well. The eye has a number of anatomical and physiological barriers against foreign species, and the majority of the drug is blinked away or wasted in tears.²⁴ The remaining drug must then penetrate the cornea and diffuse through the aqueous humor in sufficient concentrations to reach the lens. In order to achieve effective concentrations of MPG in the lens, it is necessary to prolong residence on the cornea.

1.2.3. Drug Delivery Vehicles Can Promote MPG Uptake and Efficacy. To increase drug residence time and penetration, drug delivery methods such as biocompatible polymers or gels have been explored. For example, a poloxamer gel-based drug delivery vehicle for MPG was studied in rodents.¹⁸ The drug delivery gel increased MPG residence time, allowing more the drug to penetrate the cornea, and thus delayed cataract formation significantly longer compared to MPG solution. Although they have generated a great deal of interest for ocular drug delivery,²⁵⁻²⁷ gels are not ideal agents for this purpose due to their instability under sterilization and storage conditions.²⁸⁻³⁰ In addition, as an antioxidant, MPG is prone to oxidation under these conditions. An ideal delivery platform for a thiol drug like MPG would prolong its retention on the ocular surface, augment its antioxidant properties, and protect it from premature degradation.

1.2.4. Nanodiamond Drug Delivery. Nanodiamond (ND) is a promising candidate for drug delivery due to its biocompatibility, physical properties, and customizability.³¹ Further, ND is chemically stable and does not degrade under harsh

sterilization conditions.³² Nanodiamonds are approximately spherical particles with a primary particle size of 4-6 nm, which results in specific surface areas in the range of 300-500 m²/g for adsorption or chemical binding of drugs.³³ Moreover, the surface of nanodiamond can be functionalized to suit a variety of applications.³⁴ For example, carboxylated nanodiamond (ND-COOH) can be used for the delivery of positively charged chemotherapy drugs.³⁵⁻⁴⁰ The majority of the ND-COOH surface will be negatively charged at physiological pH (7.4) due to the deprotonation of the carboxylic acid groups. The positively charged chemotherapy drug tends to remain bound to the negatively charged ND-COOH due to electrostatic interactions. Upon reaching the acidic microenvironment surrounding tumor cells, however, the negative charge on the ND-COOH will become neutralized. With electrostatic interactions greatly reduced, the drug is readily desorbed in the tumor microenvironment.

In the case of ocular drug delivery, pH-triggered release is not a primary concern. Instead, it may be useful to engineer the nanodiamond surface to maximize interactions with the cornea in order to improve residence time and resist being blinked away. Other considerations include ND loading capacity, agglomeration, rate of release, toxicity limits, and impact on drug effectiveness. Nanodiamond may also be particularly advantageous for delivery of antioxidants because they can absorb UV light, thereby preventing premature degradation of the antioxidant drug.⁴¹ Even better, some studies have shown that ND may exhibit some level of intrinsic antioxidant activity.^{41, 42}

1.3. DEVELOPMENT AND EVALUATION OF ND:MPG FORMULATIONS

The studies reported in this dissertation reflect the foundational work necessary for evaluating the potential for MPG to protect against oxidative stress and to establish and evaluate the potential of ND as an MPG delivery vehicle for the prevention of cataract and other age-related eye disorders. This dissertation reports the following three studies in greater detail:

1. The potential of MPG to protect cells from oxidative damage was evaluated in an epithelial cell line commonly used for early drug screening.
2. A high-sensitivity method was developed for quantifying MPG and its metabolite, MPA, in ocular tissues. This is a necessary tool for determining the extent of MPG loading and release from ND, as well as its fate when administered to biological models.
3. The effect of ND surface chemistry on adsorption and release of MPG was determined. This information is important for informing the selection of surface functionality in the context of different applications. The results of this study can also be used to understand why one type of ND functionalization may be more or less effective than another.

PAPER**I. PROTECTIVE EFFECTS OF TIOPRONIN ON OXIDATIVELY CHALLENGED HUMAN LUNG CARCINOMA EPITHELIAL CELLS (A549)**

Justin Beltz¹, Anna Chernatynskaya¹, Annalise Pfaff¹, Nuran Ercal^{1,*}

¹Department of Chemistry, Missouri University of Science and Technology, Rolla, MO 65409

¹J. Beltz and A. Chernatynskaya contributed equally to this work as primary authors.

*Corresponding Author

Address: 230 Schrenk Hall, 400 West 11th Street, Rolla, MO 65409

Phone: (573) 341 6950

E-mail: nercal@mst.edu

ABSTRACT

Tiopronin (MPG) is a thiol antioxidant drug that has been explored as a treatment for various oxidative stress-related disorders. However, many of its antioxidant capabilities remain untested in well-validated cell models. To more thoroughly understand the action of this promising pharmaceutical compound against acute oxidative challenge, A549 human lung carcinoma cells were exposed to *tert*-butyl hydroperoxide (*t*BHP) and treated with MPG. Analyses of cell viability, intracellular glutathione (GSH) levels, and prevalence of reactive oxygen species (ROS) and mitochondrial superoxide were used to examine the effects of MPG on *t*BHP-challenged cells. MPG treatment suppressed intracellular ROS and mitochondrial superoxide and prevented *t*BHP-induced

GSH depletion and apoptosis. These results indicate that MPG is effective at preserving redox homeostasis against acute oxidative insult in A549 cells if present at sufficient concentrations during exposure to oxidants such as *t*BHP. The effects of treatment gleaned from this study can inform experimental design for future *in vivo* work on the therapeutic potential of MPG.

Keywords: thiols, antioxidant, oxidative stress, reactive oxygen species (ROS), glutathione, tiopronin

1. INTRODUCTION

N-(2-mercaptopropionyl)glycine (MPG), or tiopronin, is low-molecular-weight thiol derivative of glycine that has been used to treat a variety of conditions. MPG was one of the first disease-modifying anti-rheumatic drugs [1-3], but it has been superseded by biologics and is now only applied in certain refractory cases [4,5]. MPG is the first-line treatment for cystinuria, in which it forms mixed disulfides that are up to 50 times more soluble than cystine, thus preventing the formation of cystine kidney stones [6,7]. While these applications fill important medicinal niches, the antioxidative properties of MPG have warranted its investigation for the treatment of more prevalent conditions. Its -SH moiety can reduce disulfide linkages between oxidized biothiols, like glutathione disulfide, restoring them to their native state [8,9]. In addition, MPG is regarded as an effective chelator of heavy metals such as mercury and copper. *In silico* models predict that formation of MPG-copper(II) complexes can reduce the rate constant of the first step in the Haber-Weiss reaction six-fold [10]. Because of these significant antioxidant

properties, MPG has been used to protect against chemotherapy-induced nephro- and hepatotoxicity [11,12], radiation poisoning [13], and ischemia-reperfusion injury to cardiac and lung tissue [12,14]. Further, MPG may be able to counteract oxidative processes that lead to lens opacification in senile cataracts [15-21]. MPG offers several advantages over similar drugs, including a more favorable side effect profile than D-penicillamine [4] and better bioavailability than *N*-acetylcysteine [22,23]. Moreover, MPG's primary metabolite, 2-mercaptopropionic acid, is also a potent radical scavenger [24]. With the growing impetus to repurpose pharmaceuticals, the medical community stands to gain potential treatments and greater understanding of oxidative stress-related conditions from renewed interest in MPG. However, its action against acute exogenous oxidative insult in cell models has not been thoroughly characterized.

To bridge this gap in understanding, well-established cell lines such as A549 are commonly used to study the action of drugs *in vitro* [25-27]. As a pulmonary epithelial cell line, it is often employed to study effects of inhalation exposure to environmental contaminants, in which oxidative stress plays a key role [28]. Further, it is recognized as a useful model for early-stage biopharmaceutical research, including studies of drug metabolism and cytotoxicity [29,30]. A well-validated oxidant is another integral component of an appropriate system for testing an antioxidant drug. For *in vitro* studies, *tert*-butyl hydroperoxide (*t*BHP) is more reliable than hydrogen peroxide, as *t*BHP has demonstrated more consistent ability to induce oxidative stress than H₂O₂ [31,32]. This may be attributed to the greater stability of the *tert*-butoxyl radical in aqueous solution [33] and fewer enzymes dedicated to its detoxification (e.g., glutathione peroxidase only versus glutathione peroxidase and catalase for H₂O₂) [25]. Further, decomposition of

*t*BHP and downstream action of its byproducts may recapitulate many of the oxidative mechanisms observed *in vivo*, including lipid peroxidation, DNA damage, depletion of GSH and protein thiols, alteration of intracellular calcium homeostasis, and apoptosis [25,34]. For these reasons, *t*BHP is better suited for probing the intracellular action of MPG. Therefore, we utilized *t*BHP to rapidly induce severe oxidative damage in A549 cells and administered MPG simultaneously to test the action of MPG against acute oxidative insult. To observe and characterize the effects of MPG under these conditions, we examined cell viability, intracellular GSH levels, and distribution of cells in apoptotic and non-apoptotic populations exhibiting intracellular ROS and mitochondrial superoxide.

2. MATERIALS AND METHODS

2.1. CHEMICALS AND REAGENTS

MPG, *t*BHP solution, Tris-HCl, L-serine, boric acid, diethylenetriaminepentaacetic acid, and *N*-(1-pyrenyl)maleimide were purchased from MilliporeSigma (St. Louis, MO). MPG stock solutions were prepared in sterile Type 1 water prepared in-house with a Millipore Simplicity 185 System. Glacial acetic acid, orthophosphoric acid, and high-performance liquid chromatography (HPLC) grade solvents were purchased from Fisher Scientific (Fair Lawn, NJ).

2.2. CELL CULTURE AND PRELIMINARY EXPERIMENTS

A549 (human lung carcinoma) cells were kindly provided by Dr. Yue-Wern Huang from the Biological Sciences Department at Missouri University of Science and Technology.

Cells were grown in phenol-red-free DMEM/F12 medium (Thermo Fisher Scientific, Waltham, MA) supplemented with 10% heat-inactivated fetal bovine serum (FBS) and 1% penicillin/streptomycin/amphotericin B (Thermo Fisher Scientific) in a humidified incubator with 5% CO₂/95% air at 37°C. Serum- and growth-factor-free medium was used for all MPG and *t*BHP experiments, instead of the fully supplemented media described above. Cells were passaged twice per week at a subcultivation ratio of 1:3. All experiments were performed using cells between passage 10 and 30.

To determine an appropriate concentration of *t*BHP for use in this study, A549 cells were seeded in multiple-well plates and divided into groups. Each group was incubated for 3 hours with a different concentration of *t*BHP in serum-free media, ranging from 0.25 mM to 4.0 mM. Cytotoxicity of *t*BHP in each group was assessed via MTT assay as described below to identify the range of concentrations at which cell viability was reduced to 50-60% of the control, which was shown to be 0.5 to 1.0 mM. To determine whether cells received sufficient oxidative insult, intracellular GSH levels were measured in groups treated with *t*BHP concentrations ranging from 0.4 to 0.8 mM for 3 hours. Based on these preliminary experiments, a concentration of 0.6 mM *t*BHP was selected for use in the remaining experiments.

Next, an appropriate concentration of MPG for treating *t*BHP-exposed cells was selected. To determine whether MPG alone had any adverse effect on cell viability,

A549 cells were seeded in multiple-well plates and divided into groups. Each group was incubated for 3 hours with different concentrations of MPG in serum-free media, ranging from 0.08 mM to 10 mM, and MPG was not found to significantly affect cell viability at these concentrations (data not shown). To determine an appropriate concentration for use in *t*BHP-exposed cells, a similar experiment was conducted with the simultaneous addition of 0.6 mM *t*BHP and either 1.0, 1.5, 2.5, or 5.0 mM MPG for 3 hours. Cell viability and GSH levels in respective groups indicated that 5.0 mM MPG provided optimal protection against *t*BHP. Based on these preliminary experiments, 5.0 mM MPG and 0.6 mM *t*BHP were used in subsequent experiments to determine the effects of MPG on oxidative stress induced by *t*BHP.

2.3. EXPERIMENTAL DESIGN

The A549 cells were grown in complete media and allowed to proliferate for 24 hours. The cells were divided into 4 treatment groups: control, MPG only, *t*BHP only, and MPG + *t*BHP. After the 24-hour proliferation time, the complete medium was removed and replaced with the treatment medium associated with the corresponding treatment group (Table 1). The treatment media were supplemented with *t*BHP or MPG immediately prior to each experiment from freshly prepared concentrated stock solutions. The cells were allowed to incubate in the treatment media for 3 hours. After this time, the treatment media were removed. Cell viability and oxidative stress parameters including GSH and flow cytometric analysis of ROS and mitochondrial superoxide were determined after treatment as described in the following sections.

Table 1. Treatment media compositions

Group	Treatment medium
Control	Medium
MPG only	Medium + 5 mM MPG
<i>t</i> BHP only	Medium + 0.6 mM <i>t</i> BHP
MPG + <i>t</i> BHP	Medium + 5 mM MPG + 0.6 mM <i>t</i> BHP

2.4. CELL VIABILITY

Cells were seeded at a density of 2×10^4 cells/well in 96-well plates and allowed to adhere and proliferate for 24 hours. Then, cells were divided into groups and treated as described in the experimental design. After the treatment, the treatment media were replaced with fresh F12 medium, and cell viability was determined using the Vybrant MTT Cell Proliferation Assay Kit (Invitrogen, Carlsbad, CA) as described by the manufacture. The MTT assay is a colorimetric assay through which cell viability is estimated by conversion of the water soluble MTT (3-(4,5-dimethylthiazol-2-yl)-2,5-dimethyltetrazolium bromide) to an insoluble formazan by viable cells. The formazan is then solubilized by sodium dodecyl sulfate (SDS), and the concentration is determined by measuring absorbance at 570 nm using a microplate reader (Fluor Star Optima, BMG, Labtech). Cell viability was expressed as the absorbance by the contents of a given well divided by that of the mean absorbance measured for the control group.

2.5. QUANTIFICATION OF INTRACELLULAR GSH LEVEL

Cells were seeded at a density of 6×10^5 cells/well in 6-well plates 24 hours before the experimental treatment. Cells were treated as described in the experimental design. Following treatment, the cells were harvested with trypsin/EDTA and collected in

1.5 mL RINO tubes (Next Advance, Troy, NY, USA). The cell suspensions were centrifuged at $500 \times g$ for 10 min at 4°C . The supernatants were removed, and the cells were resuspended in 1 mL aliquots of PBS to rinse away remaining media and extracellular GSH. This centrifugation and rinsing process was repeated. After rinsing, the cells were centrifuged again at $500 \times g$ and resuspended in 250 μL aliquots of chilled serine-borate buffer (100 mM Tris-HCl, 5 mM L-serine, 10 mM boric acid, 1 mM diethylenetriaminepentaacetic acid, pH 7.0). A 100 μL scoop was used to add about 100 μL of zirconium oxide beads (0.5 mm diameter, Next Advance) to each of the cell suspensions. The cells were homogenized using a Bullet Blender Storm tissue homogenizer (Next Advance) at speed “8” for 3 min. After homogenization, the cells were immediately centrifuged at $5000 \times g$ for 5 min at 4°C . Then, 100 μL aliquots of supernatant were collected from each RINO tube for analysis of GSH and total protein content.

Intracellular GSH levels were determined by HPLC with pre-column derivatization and fluorescence detection, according to a method developed in our laboratory [35]. Briefly, 50- μL aliquots of cell homogenate were diluted with 200 μL of serine-borate buffer. The samples were derivatized by the addition of 750 μL of *N*-(1-pyrenyl)maleimide (1 mM in acetonitrile). The samples were mixed and allowed to react for 5 min. After this time, 10 μL of 2 M HCl were added to stabilize the fluorescent adducts. Samples were filtered with 0.45 μm nylon membrane filters. Samples were injected onto an Orochem (Naperville, IL, USA) Reliasil ODS-1 column (4.6 mm i.d. \times 250 mm) and eluted with a mobile phase consisting of 70:30 (v/v) acetonitrile-water with 1 mL/L of *o*-phosphoric acid and 1 mL/L of glacial acetic acid, delivered at a flow rate of

1 mL/min. GSH levels were determined by using a calibration curve prepared from standards processed in parallel with the unknown samples.

The GSH levels were normalized to the amount of total protein present in each sample. Total protein levels were estimated using the Coomassie dye-binding method described by Bradford [36]. Bradford dye reagent (Bio-Rad, Hercules, CA, USA) was diluted five-fold in serine borate buffer, and 1 mL aliquots of the diluted dye reagent were added to 20 μ L of diluted cell homogenate in cuvettes. The samples were left to incubate at room temperature for at least 5 min. The absorbance of 595 nm light was correlated to the total protein concentration using a calibration curve. Albumin from bovine serum was used to make calibration standards to estimate the protein content in the cell homogenates.

To account for differences in live cell populations between treatment groups, GSH levels were reported in nanomoles of GSH per milligram of protein (nmol/mg).

2.6. FLOW CYTOMETRY ANALYSIS OF APOPTOTIC CELLS AND INTRACELLULAR ROS MEASUREMENT

Intracellular ROS content was measured using the carboxy derivative of fluorescein, carboxy-H₂DCFDA (6-carboxy-2',7'-dichlorofluorescein diacetate, Molecular Probes, Invitrogen), due to its additional negative charges that enhance cellular retention [37]. Flow cytometry (BD Accuri C6, BD Biosciences, Ann Arbor, MI) was used to assess the distribution of cells that contained ROS (ROS⁺ cells) within apoptotic and non-apoptotic cell populations. Cells were seeded on 24-well plates (Corning) at a density of 2×10^5 cells/well, grown over 24 hours, divided into groups and dosed as described previously. Trypsinized cells were washed with PBS and re-suspended in 250

μL of PBS containing $10 \mu\text{M}$ carboxy- H_2DCFDA . After incubation for 30 minutes at 37°C , the cells were washed with annexin V binding buffer and stained with 7-AAD (7-aminoactinomycin D, BD Pharmingen) and Annexin V Alexa Fluor 647 Conjugate (Invitrogen) for 15 minutes at room temperature in the dark. The FL-1 channel ($\lambda_{\text{ex}} = 488 \text{ nm}$ and $\lambda_{\text{em}} = 533 \text{ nm}$) was used for carboxy- H_2DCFDA , and the FL-3 channel ($\lambda_{\text{ex}} = 533 \text{ nm}$ and $\lambda_{\text{em}} = 670 \text{ nm}$) was used for 7-AAD. Annexin V Alexa Fluor 647 fluorescence was measured using the FL-4 channel ($\lambda_{\text{ex}} = 640 \text{ nm}$ and $\lambda_{\text{em}} = 675 \text{ nm}$). Debris were excluded by forward vs. side scatter gating. Results are reported as percent of total cell population.

2.7. FLOW CYTOMETRY DETERMINATION OF MITOCHONDRIAL SUPEROXIDE

MitoSOX Red mitochondrial superoxide indicator (MSR) is a fluorogenic dye for selective detection of superoxide in mitochondria of live cells (Molecular Probes, Eugene, OR). MSR is a dihydroethidium dye with a lipophilic, positively-charged side-chain for targeted absorption by the mitochondria. Upon oxidation by superoxide, the dye exhibits red fluorescence [38]. For analysis of superoxide generated in mitochondria, cells were grown in the same conditions as for the measurement of ROS content via flow cytometer. Harvested cells were washed with PBS and re-suspended in $250 \mu\text{L}$ of PBS containing $5 \mu\text{M}$ MSR. Cells were incubated for 30 minutes at 37°C . After incubation with MSR, LIVE/DEAD Fixable Green Dye (Molecular Probes, Eugene, OR) was added directly to each sample according to the manufacture's recommendation. Cells were incubated for an additional 15 minutes at room temperature. The final stain, Annexin V Alexa Fluor 647 Conjugate, was added after washing cells with annexin V buffer. Cells

were analyzed by flow cytometry using the FL-1 channel ($\lambda_{\text{ex}} = 488 \text{ nm}$ and $\lambda_{\text{em}} = 533 \text{ nm}$) for LIVE/DEAD Fixable Green, the FL-2 channel for MSR ($\lambda_{\text{ex}} = 488 \text{ nm}$ and $\lambda_{\text{em}} = 585 \text{ nm}$), and the FL-4 channel for Annexin-V Alexa Fluor 647 ($\lambda_{\text{ex}} = 640 \text{ nm}$ and $\lambda_{\text{em}} = 675 \text{ nm}$). Results are reported as percent of total cell population with MSR fluorescence (MSR+) cells in apoptotic and viable populations in each treatment group. Debris were excluded by forward vs. side scatter gating.

2.8. STATISTICAL ANALYSIS

Statistical analysis was performed using GraphPad Prism 8 software (GraphPad, San Diego, CA, USA). All values were reported as mean \pm standard deviation of at least three separate experiments, with $n = 3\text{--}16$. Statistical significance was performed by two-way analysis of variance (ANOVA) for flow cytometry experiments and one-way ANOVA for all other experiments. ANOVA was followed by Tukey's or Dunnett's multiple comparison tests.

3. RESULTS AND DISCUSSION

3.1. SELECTION OF DOSING CONCENTRATIONS

To determine an appropriate concentration of tBHP for inducing oxidative stress, cell viability and GSH levels were determined following exposure to varied concentrations of tBHP. GSH, γ -glutamyl-cysteinyl-glycine, is the most abundant non-protein thiol in the body and an essential endogenous antioxidant. It plays a vital role in reduction and detoxification of ROS, including peroxides like tBHP and is therefore crucial to the maintenance of redox homeostasis. Increase in oxidants can upset this

delicate balance, leading to the oxidative modification of critical cellular components, dysfunction, and ultimately apoptosis. The effects of increasing *t*BHP concentrations on cell viability and GSH levels are reported in Figure 1. Concentrations from 0.25 mM to 4.0 mM significantly decreased cell viability in a dose-dependent manner. The effect of *t*BHP concentration on GSH levels and cell morphology were also considered for selection of an appropriate concentration of *t*BHP for subsequent experiments. *t*BHP concentrations from 0.4 mM to 0.8 mM resulted in a statistically significant decrease in levels of intracellular GSH, which correlates with the dose-dependent decrease in cell viability.

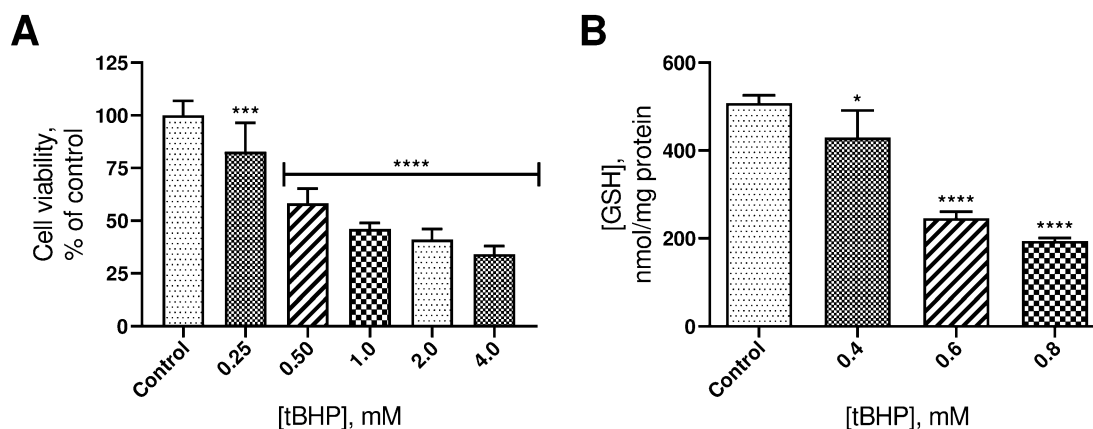


Figure 1. A. Plot of cell viability vs. *t*BHP concentration. The height of the columns indicates the mean viability from 9 experiments. Error bars indicate standard deviation. B. Plot of intracellular GSH concentration vs. *t*BHP concentration. The height of the columns represents the mean of 3 experiments. Error bars indicate standard deviation. **** $p \leq 0.0001$ compared to control. *** $p \leq 0.001$ compared to control. * $p \leq 0.05$ compared to control.

Upon comparing the effects of *t*BHP on GSH levels and cell morphology, it was noted that at 0.6 mM *t*BHP, GSH had decreased by approximately 50%, but at 0.8 mM,

cells lost adhesion, which interfered with analysis and weakened integrity of the model overall. A *t*BHP concentration of 0.6 mM struck the best balance between oxidative damage and maintenance of normal cell morphology. Therefore, 0.6 mM *t*BHP was selected for subsequent experiments. Although this *t*BHP concentration is relatively high, the A549 cell line is reportedly resistant to oxidative insult [39].

In the next set of experiments, a variety of MPG concentrations from 1.0 to 5.0 mM were tested in different groups to determine the appropriate concentration for protection against oxidative stress induced by 0.6 mM *t*BHP. Intracellular GSH levels were used to assess the effectiveness of each dose, and the results are shown in Figure 2.

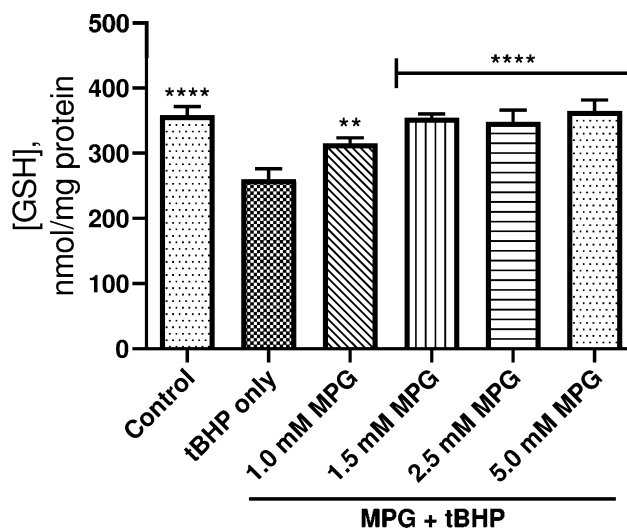


Figure 2. Plot of intracellular GSH concentration vs. dosing concentration of MPG. The height of the columns represents the mean of 3 experiments. Error bars indicate standard deviation. **** $p \leq 0.0001$ compared to *t*BHP only. ** $p \leq 0.01$ compared to *t*BHP only.

Concentrations ranging from 1.0 mM to 5.0 mM MPG afforded significant improvement in GSH levels compared to untreated, *t*BHP-exposed cells, but cells treated

with 5.0 mM MPG exhibited the highest GSH levels. Since preliminary experiments showed concentrations of MPG up to 10 mM to be nontoxic to A549 cells, treatment with 5.0 mM MPG was deemed an appropriate treatment for *t*BHP-induced oxidative stress for the remainder of the study.

3.2. EFFECT OF MPG ON INTRACELLULAR GSH IN OXIDATIVELY CHALLENGED A549 CELLS

To confirm the effects of 5.0 mM MPG on intracellular GSH levels in A549 cells, the cells were divided into groups as discussed in the experimental design and seeded as described earlier. The results of the intracellular GSH analyses are reported in Figure 3A. The data were normalized by the amount of protein present in each sample to account for differences in viable cell count. Exposure to *t*BHP without MPG resulted in a significant decrease in intracellular GSH levels compared to the control group. Cells treated with MPG, either with or without *t*BHP, had GSH levels that were not significantly different from that of the control group. Therefore, administration of 5.0 mM MPG with 0.6 mM *t*BHP was effective for preventing loss of free GSH, and MPG alone does not increase GSH levels beyond that of the control group. These results are consistent with the hypothesis that GSH levels are spared by the action of MPG as opposed to being directly increased.

3.3. EFFECT OF MPG ON VIABILITY OF OXIDATIVELY CHALLENGED A549 CELLS

To determine whether MPG could protect cells from *t*BHP-induced loss of viability, the MTT assay was used as an indicator of cellular metabolism. This assay is

based on the ability of metabolically active cells to reduce MTT to an insoluble, colored formazan product that can be measured spectrophotometrically. Cell viability for each treatment group is reported in Figure 3B as a percentage of absorbance at 570 nm compared to that of the control group. As was the case in our preliminary studies, cells exposed to 0.6 mM *t*BHP without MPG exhibited significantly less viability compared to the cells in the control group, and the viability of cells in the MPG + *t*BHP group was statistically similar to that of the cells in the control group. Treatment of A549 with 5 mM MPG alone also did not increase or decrease cell viability.

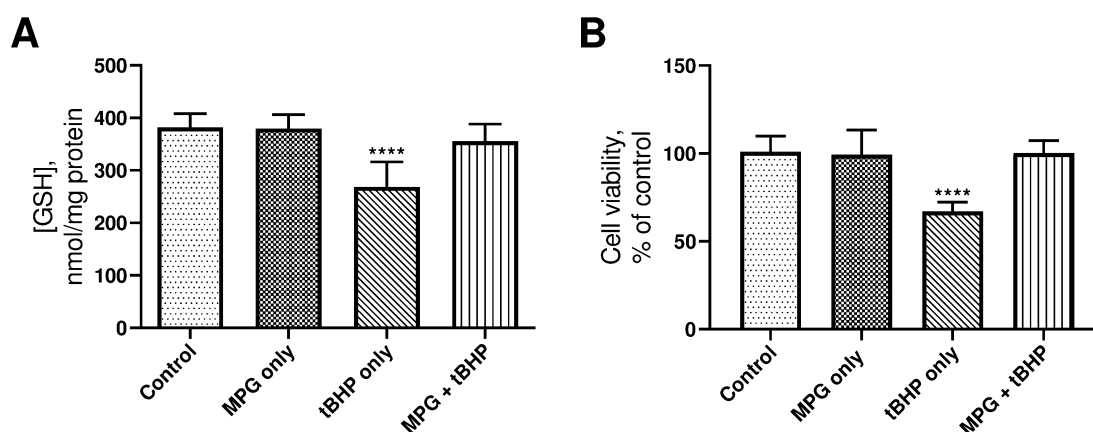


Figure 3. A. Plot of treatment vs. intracellular GSH concentration. The height of the columns indicates the mean of 9 experiments and error bars represent the standard deviation. B. Plot of treatment vs. cell viability. The height of the columns indicates the mean of 14 experiments, and error bars represent the standard deviation. **** $p \leq 0.0001$ compared to control.

This trend closely parallels that of intracellular GSH levels and makes sense in the context of the biochemistry behind the MTT assay. The reduction of MTT to formazan is sensitive to decreases in available NADPH [40]. The NADPH cofactor serves as the reductant for a host of anabolic processes, as well as the reduction of oxidized glutathione

to its active reduced form. Thus, gross metabolic dysfunction resulting from *t*BHP is manifested in the inability of oxidatively damaged, dying cells to reduce MTT and regenerate GSH from its oxidized form. In contrast, cells treated with MPG exhibited marked improvement in both cell viability and GSH levels. We hypothesize that this is due to the following effects of MPG. As a thiol antioxidant that can directly reduce *t*BHP-derived ROS, MPG can spare GSH from oxidation, leaving cellular GSH stores largely intact. In preventing oxidation of GSH, MPG also preserves NADPH for use in reductive biosynthesis and conversion of MTT to formazan.

3.4. EFFECT OF TREATMENT ON APOPTOTIC AND NECROTIC CELL POPULATIONS

Flow cytometry is a well-established technology that has been widely used for measuring intrinsic and extrinsic properties of fluorescently labeled cells. This property permits the identification of subpopulations within the sample, and quantification of cell populations through selective fluorescence labeling. While microplate readers provide rapid data acquisition, the accuracy of the measurements suffers since the end value corresponds to the average fluorescence per well while flow cytometry provides information at the single-cell level. For this analysis, cells were labeled with 7-AAD and Annexin V Alexa 647 to investigate live, necrotic, and apoptotic cell populations. Live cells are not typically permeable to 7-AAD. Cells in early apoptotic stages bind only to Annexin V Alexa 647, while cells in late apoptotic stages bind to both Annexin V Alexa 647 and 7-AAD. Necrotic cells bind to 7-AAD, but not Annexin V Alexa 647.

Representative dot-plots from the flow cytometry analysis are provided in Figure 4. The mean distributions of cells among apoptotic, necrotic, and viable cell populations from 8 replicate experiments are summarized in Table 2.

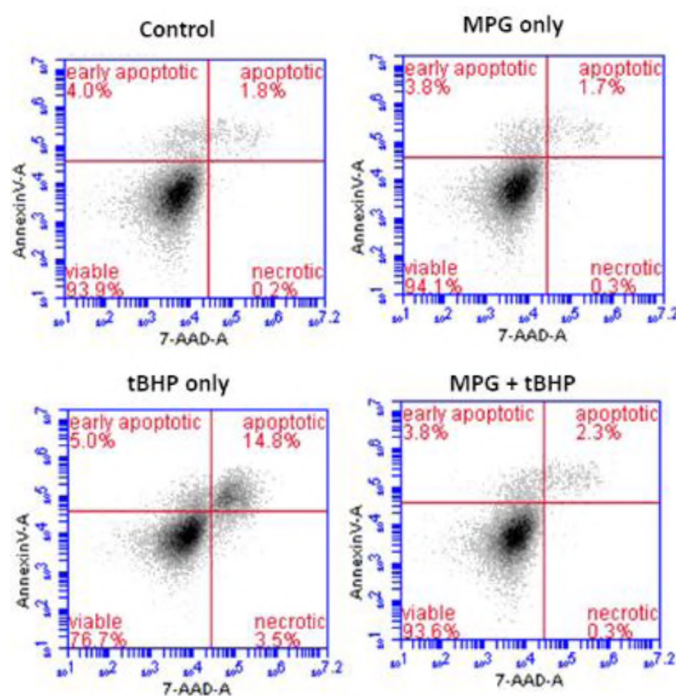


Figure 4. Representative dot-plots from flow cytometry analysis of apoptotic cells. Shown are plots of fluorescence associated with Annexin V Alexa 647 (FL-4) vs. 7-AAD (FL-3) from different treatment groups.

Table 2. Effects of exposure to *t*BHP and treatment with MPG on viable, apoptotic, and necrotic subpopulations.

Subpopulation	Cells in subpopulation (% of total cell population) [†]			
	Control	MPG only	<i>t</i> BHP only	MPG + <i>t</i> BHP
Early apoptotic	3.1 ± 1.3	2.6 ± 0.9	4.3 ± 1.3	3.0 ± 0.7
Late apoptotic	2.3 ± 0.4****	2.3 ± 0.6****	11.2 ± 4.7	2.9 ± 0.7****
Viable	94.3 ± 1.2****	94.5 ± 0.8****	81.7 ± 8.2	93.5 ± 1.0****
Necrotic	0.4 ± 0.3	0.6 ± 0.4	2.8 ± 2.6	0.6 ± 0.6

[†] Mean ± SD of 8 experiments.

**** $p \leq 0.0001$, compared to *t*BHP only group.

As observed previously, the percentage of viable cells in the MPG + tBHP treated group was significantly higher than in the tBHP group. Further, the percentage of viable cells in the MPG + tBHP group was statistically similar to the percentages in the MPG only group and the control group. The same trend was observed within late apoptotic subpopulations. Exposure to 0.6 mM tBHP without MPG resulted in an elevated proportion of cells exhibiting fluorescence associated with binding of 7-AAD and Annexin V Alexa 647. However, cells treated with MPG, alone or with tBHP, were not significantly different from the control cells. These data suggest that exposure to 0.6 mM tBHP without MPG results in oxidative stress-associated apoptosis while treatment with MPG mitigates the damage that triggers this process. Although there does not appear to be a significant difference in the proportion of cells occupying the necrotic quadrant among groups, this can be attributed to the fact that cellular debris are excluded prior to quantitation. There was a significantly lower number of cells available for counting in the tBHP only group, compared to the other groups. This loss of countable cells is indicative of membrane disintegration associated with tBHP exposure.

3.5. DISTRIBUTION OF CELLS WITH ROS PRESENT IN APOPTOTIC AND NON-APTOPTOTIC SUBPOPULATIONS

Based on the results of GSH and MTT assays, we hypothesized that MPG prevents cell death by protecting cells from oxidative damage, and therefore, we would expect to see significantly higher levels of ROS in cells in the tBHP only group than in the other groups. To estimate the levels of intracellular ROS, carboxy-H₂DCFDA was used to identify ROS⁺ cells. Carboxy-H₂DCFDA is a membrane-permeable derivative of the fluorescent probe fluorescein. Upon cleavage of its acetate groups and oxidation by

intracellular ROS, the dye becomes trapped within the cell and fluoresces green [38]. Cells were co-stained with two other fluorescent probes, Annexin V Alexa Fluor 647 conjugate and 7-AAD, and then the cells were subjected to flow cytometric analysis. Representative dot plots are shown in Figure 5. In this study, co-staining was used to differentiate between apoptotic and non-apoptotic cell subpopulations and to exclude necrotic cells since membrane leakage makes estimation of intracellular ROS unreliable.

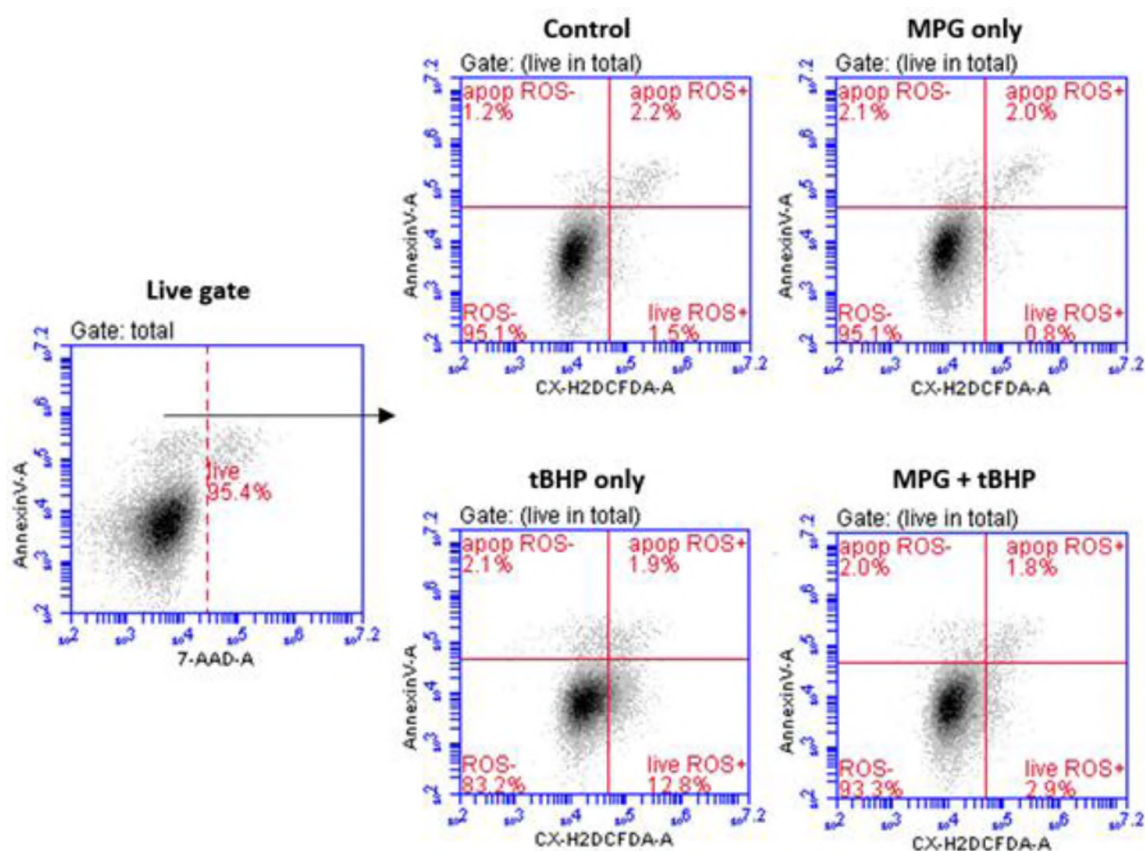


Figure 5. Representative dot-plots from flow cytometry analysis of ROS in apoptotic and live subpopulations. The cells were gated excluding debris. Viable cells were gated by exclusion of 7-AAD+ cells (FL-3) on 2D plots (live gate). The quantification of ROS was done using 2D plots of Carboxy-H₂DCFDA (FL-1) vs. Annexin V Alexa 647 (FL-4).

Table 3. Effects of *t*BHP exposure and MPG treatment on percentage of ROS+ cells in apoptotic and live cell populations.

Subpopulation	Cells in subpopulation (% of total cell population) [†]			
	Control	MPG only	<i>t</i> BHP only	MPG + <i>t</i> BHP
ROS in apoptotic cells	1.7 ± 0.9	1.3 ± 0.8	3.6 ± 1.4	1.6 ± 0.6
ROS in live cells	1.5 ± 0.5****	2.2 ± 1.1****	22.5 ± 2.3	4.2 ± 1.0****
Total ROS	3.3 ± 0.9****	3.5 ± 1.6****	26.1 ± 2.7	5.8 ± 1.1****

[†] Mean ± SD of 8 experiments.

**** $p \leq 0.0001$, compared to *t*BHP only group.

The results of the analysis (summarized in Table 3) indicate that there were indeed significantly more ROS detected in live cells treated with *t*BHP only than in any of the other groups. This correlates well with the GSH and cell viability results and is consistent with the supposition that MPG protects cells from oxidative stress by reducing ROS associated with exposure to *t*BHP.

Numbers of ROS+ cells in apoptotic subpopulations were low in all groups, and differences between these subpopulations did not reach statistical significance. Small subpopulations of apoptotic, ROS+ cells may be due to the exclusion of late-stage apoptotic and necrotic cells by gating out 7-AAD-fluorescent cells. As shown in Table 2, the *t*BHP only group had a significantly higher subpopulation of late-stage apoptotic cells, suggesting that *t*BHP-induces rapid progression to late-stage apoptosis or secondary necrosis [41]. Since these cells exhibit 7-AAD fluorescence, they would have been gated out and thereby excluded from the study [42].

3.6. DISTRIBUTION OF SUPEROXIDE PRESENT IN MITOCHONDRIA OF APOPTOTIC AND NON-APOPTOTIC POPULATIONS

Low levels of superoxide in mitochondria are generated as a result of normal metabolic processes, but excessive amounts are associated with electron-transport chain

dysfunction [43]. This can lead to decreased ATP production, loss of mitochondrial membrane potential, and ultimately opening of the mitochondrial permeability transition pore and initiation of the apoptotic cascade [44,45]. In this way, mitochondria are highly sensitive to fluctuations in redox status, [44] and may serve as a predictor of apoptotic response to acute oxidative insult [45].

MSR, a mitochondria-permeable dye, fluoresces upon oxidation by superoxide. Similar to the flow cytometric analysis of ROS⁺ cells, MSR was used to determine the percentage of cells with superoxide present in the mitochondria. Representative dot plots are shown in Figure 6.

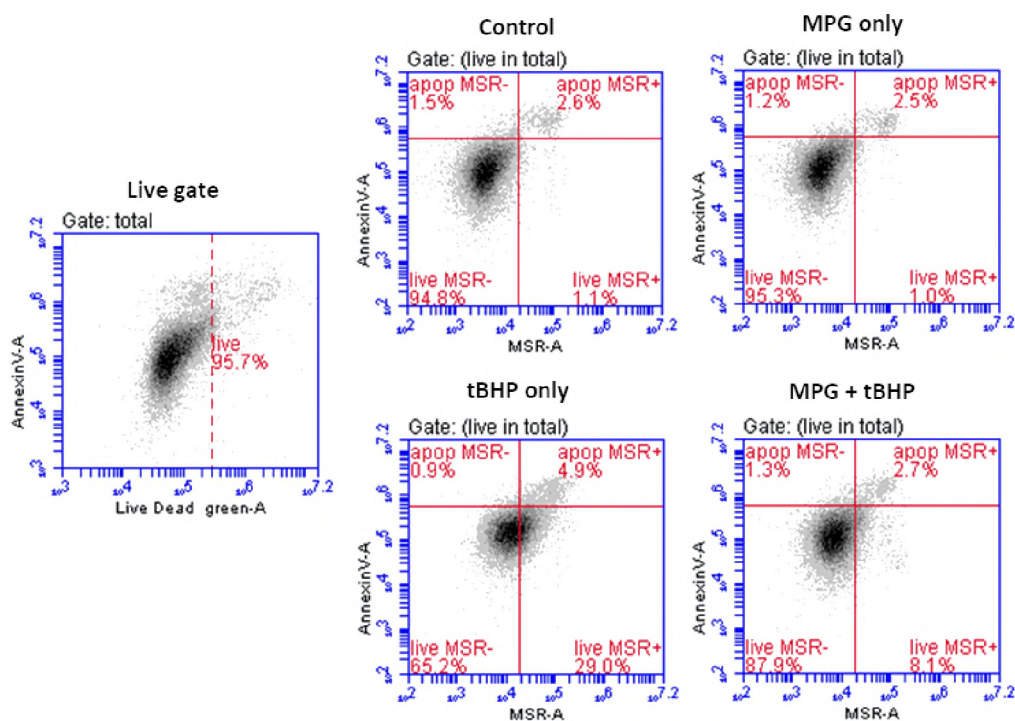


Figure 6. Representative dot-plots of from flow cytometry analysis of superoxide in mitochondria. The total cells were gated excluding debris. Viable cells were gated by exclusion of Live/Dead green⁺ cells (FL-1) on 2D plots (live gate). The quantification of MSR⁺ cells was done using 2D plots of MSR (FL-2) vs. Annexin V Alexa 647 (FL-4).

Table 4 shows the quantitative results as mean percentages of the total cell population. The percentage of MSR+ live cells in the MPG + tBHP group was significantly decreased compared to that in the tBHP only group. This indicates that MPG was able to preserve mitochondrial redox status. In light of the cell viability and GSH results, it may be the case that MPG prevents downstream release of mitochondria-derived ROS into the cell and halts progression towards apoptosis.

Table 4. Effects of exposure to tBHP and MPG on the percentage of MSR+ cells in apoptotic and live cell populations.

Subpopulation	Cells in subpopulation (% of total cell population) [†]			
	Control	MPG only	tBHP only	MPG + tBHP
MSR+ in apoptotic cells	2.1 ± 0.5	2.0 ± 0.4	3.9 ± 1.3	2.3 ± 0.5
MSR+ in live cells	1.2 ± 0.4****	1.3 ± 0.3****	24.3 ± 3.2	8.6 ± 1.9****
Total MSR+ cells	3.2 ± 0.8****	3.5 ± 0.5****	28.2 ± 3.5	10.9 ± 2.2****

[†] Mean ± SD of 8 experiments.

**** $p \leq 0.0001$, compared to tBHP only group.

4. CONCLUSIONS

In this study, tBHP was used to induce oxidative stress in A549 cells. Cells exposed to 0.6 mM tBHP without MPG showed elevated levels of intracellular ROS, mitochondrial superoxide, and cell death while also showing reduced levels of the vital antioxidant GSH and reduced cell viability. When 5.0 mM MPG was present along with 0.6 mM tBHP, normal levels of these oxidative stress parameters were maintained. It is likely that MPG is interacting as a direct ROS scavenger, and the results obtained through this study suggest that if MPG is present in sufficiently high concentrations during an oxidative insult, it can be highly effective at preventing the ensuing damage. It is

probable that the MPG reacts directly with *t*BHP in the treatment medium, reducing it and its oxidative byproducts before they can cause significant damage to the cells. This action is desirable for treatment applications which demand protection against acute oxidative insult such as radioprotection, but it is important to consider the dosing conditions and timing since biological systems are inherently dynamic. This *in vitro* system lacks many of the complexities of *in vivo* models and is therefore subject to some limitations. Due to the robust nature of this lung carcinoma cell line, a relatively high dose of *t*BHP was required to model acute oxidative stress. Despite the popularity of this approach, it may not directly translate to *in vivo* systems. Thus, the results of this study warrant further investigation in more representative models, such as primary cell cultures and eventually animal studies.

ACKNOWLEDGMENTS

The authors would like to thank Alex Cristea for his assistance in conducting preliminary work and GSH analysis.

FUNDING DETAILS

This work was supported by the Richard K. Vitek/FCR Endowment in Biochemistry at Missouri University of Science and Technology and the NEI of the National Institutes of Health under award number R15EY029813.

DISCLOSURE STATEMENT

The authors report no conflict of interest.

DATA AVAILABILITY STATEMENT AND DATA DEPOSITION

The data generated from the current study are available from the corresponding author on reasonable request.

REFERENCES

1. Wood PL, Khan MA, Moskal JR. Mechanism of action of the disease-modifying anti-arthritic thiol agents D-penicillamine and sodium aurothiomalate: restoration of cellular free thiols and sequestration of reactive aldehydes. *Eur J Pharmacol.* 2008 Feb 2;580(1-2):48-54.
2. Pasero G, Pellegrini P, Ambanelli U, et al. Controlled multicenter trial of tiopronin and D-penicillamine for rheumatoid arthritis. *Arthritis Rheum.* 1982 Aug;25(8):923-9.
3. Amor B, Mery C, Gery AD. Tiopronin (N-[2-mercaptopropionyl] glycine) in rheumatoid arthritis. *Arthritis Rheum.* 1982;25(6):698-703.
4. Jaffe IA. Adverse effects profile of sulfhydryl compounds in man. *Am J Med.* 1986 Mar;80(3):471-6.
5. Czlonkowska A, Litwin T. Wilson disease - currently used anticopper therapy. *Handb Clin Neurol.* 2017;142:181-191.
6. Fjellstedt E, Denneberg T, Jeppsson J-O, et al. Cystine analyses of separate day and night urine as a basis for the management of patients with homozygous cystinuria. *Urol Res.* 2001;29(5):303-310.
7. Joly D, Rieu P, Mejean A, et al. Treatment of cystinuria. *Pediatr Nephrol.* 1999 Nov;13(9):945-50.

8. Okumura S, Toshioka N, Asakura S, et al. Studies on the oxidation-reduction potentials of 2-mercaptopropionylglycine and penicillamine using thiol-disulfide exchange reactions with cysteine and glutathione. *Yakugaku Zasshi*. 1974;94(6):655-659.
9. Wood PL, Khan MA, Moskal JR. Cellular thiol pools are responsible for sequestration of cytotoxic reactive aldehydes: central role of free cysteine and cysteamine. *Brain Res*. 2007 Jul 16;1158:158-63.
10. Castañeda-Arriaga R, Vivier-Bunge A, Raul Alvarez-Idaboy J. Primary antioxidant and metal-binding effects of tiopronin: A theoretical investigation of its action mechanism. *Comput Theor Chem*. 2016;1077:48-57.
11. Zhang JG, Lindup WE. Tiopronin protects against the nephrotoxicity of cisplatin in rat renal cortical slices in vitro. *Toxicol Appl Pharmacol*. 1996 Dec;141(2):425-33.
12. Atmaca G. Antioxidant effects of sulfur-containing amino acids. *Yonsei Med J*. 2004 Oct 31;45(5):776-88.
13. Devi PU, Saharan BR. Chemical protection of mouse spermatocytes against gamma-rays with 2-mercaptopropionylglycine. *Experientia*. 1978 Jan 15;34(1):91-2.
14. Date M-o, Morita T, Yamashita N, et al. The antioxidant N-2-mercaptopropionyl glycine attenuates left ventricular hypertrophy in in vivo murine pressure-overload model. *J Am Coll Cardiol*. 2002;39(5):907-912.
15. Abdelkader H, Alany RG, Pierscionek B. Age-related cataract and drug therapy: opportunities and challenges for topical antioxidant delivery to the lens. *J Pharm Pharmacol*. 2015 Apr;67(4):537-50.
16. Peng Y-S, Zhang J, Zhao W-J, et al. Inhibitory effect of tiopronin on hydrogen dioxide induced cataract in rabbit. *Yanke Xinjinzhan*. 2009 Feb;29(2).
17. Kobayashi S, Kasuya M, Ishii Y, et al. Effects of 2-mercaptopropionylglycine on the development of X-ray-induced cataract in rats. *Curr Eye Res*. 1992 Nov;11(11):1099-103.
18. Ichikawa H, Imaizumi K, Tazawa Y, et al. Effect of tiopronin on senile cataracts. A double-blind clinical study. *Ophthalmologica*. 1980;180(5):293-8.
19. Nishigori H, Hayashi R, Lee JW, et al. Effect of MPG on glucocorticoid-induced cataract formation in developing chick embryo. *Invest Ophthalmol Vis Sci*. 1984 Sep;25(9):1051-5.

20. Jiang T-Y, Sun C-S, Shen X, et al. Development of a poloxamer analogs/bioadhesive polymers-based in situ gelling ophthalmic delivery system for tiopronin. *J Appl Polym Sci*. 2009;114(2):775-783.
21. Kuck JF, Jr., Kuck KD. The Emory mouse cataract: the effects on cataractogenesis of alpha-tocopherol, penicillamine, triethylenetetramine, and mercaptopropionylglycine. *J Ocul Pharmacol*. 1988 Fall;4(3):243-51.
22. Olsson B, Johansson M, Gabrielsson J, et al. Pharmacokinetics and bioavailability of reduced and oxidized N-acetylcysteine. *Eur J Clin Pharmacol*. 1988;34(1):77-82.
23. Carlsson MS, Denneberg T, Emanuelsson BM, et al. Pharmacokinetics of oral tiopronin. *Eur J Clin Pharmacol*. 1993;45(1):79-84.
24. Beltz J, Pfaff A, Ercal N. Simultaneous determination of tiopronin and its primary metabolite in plasma and ocular tissues by HPLC. *Biomed Chromatogr*. 2018 Sep 3:e4375.
25. Alia M, Ramos S, Mateos R, et al. Response of the antioxidant defense system to tert-butyl hydroperoxide and hydrogen peroxide in a human hepatoma cell line (HepG2). *J Biochem Mol Toxicol*. 2005;19(2):119-28.
26. Unger RE, Pohl C, Hermanns I, et al. Cell culture systems for studying biomaterial interactions with biological barriers. *Methods of Analysis. Comprehensive Biomaterials*. Vol. 1: Elsevier; 2011.
27. Ehrhardt C, Laue M, Kim K-J. In vitro models of the alveolar epithelial barrier. In: Ehrhardt C, Kim K-J, editors. *Drug Absorption Studies: In Situ, In Vitro And In Silico Models*. Biotechnology: Pharmaceutical Aspects: Springer US; 2008.
28. Hsu HT, Tseng YT, Wong WJ, et al. Resveratrol prevents nanoparticles-induced inflammation and oxidative stress via downregulation of PKC-alpha and NADPH oxidase in lung epithelial A549 cells. *BMC Complement Altern Med*. 2018 Jul 9;18(1):211.
29. Buckley ST, Kim K-J, Ehrhardt C. In vitro cell culture models for evaluating controlled release pulmonary drug delivery. In: Smyth HDC, Hickey AJ, editors. *Controlled Pulmonary Drug Delivery. Advances in Delivery Science and Technology*: Springer-Verlag New York; 2011.
30. Constant S, Wiszniewski L, Huang S. The use of in vitro 3D cell models of human airway epithelia (MucilAir(TM)) in inhalation technology. In: Haycock JW, Ahluwalia A, Wilkinson JM, editors. *Cellular In Vitro Testing: Methods and Protocols*: CRC Press, Taylor & Francis Group; 2014.

31. Walther UI, Stets R. Glucocorticoid pretreatment increases toxicity due to peroxides in alveolar epithelial-like cell lines. *Toxicology*. 2009;256(1-2):48-52.
32. Dierickx PJ, Van Nuffel G, Alvarez I. Glutathione protection against hydrogen peroxide, tert-butyl hydroperoxide and diamide cytotoxicity in rat hepatoma-derived Fa32 cells. *Hum Exp Toxicol*. 1999;18(10):627-633.
33. Pryor Wa. OXY-RADICALS AND RELATED and Reactions. *Annu Rev Physiol*. 1986;48:657-667.
34. Altman SA, Zastawny TH, Randers L, et al. tert.-butyl hydroperoxide-mediated DNA base damage in cultured mammalian cells. *Mutat Res*. 1994 Apr 1;306(1):35-44.
35. Ates B, Ercal BC, Manda K, et al. Determination of glutathione disulfide levels in biological samples using thiol-disulfide exchanging agent, dithiothreitol. *Biomed Chromatogr*. 2009 Feb;23(2):119-23.
36. Bradford MM. A rapid and sensitive method for the quantitation of microgram quantities of protein utilizing the principle of protein-dye binding. *Anal Biochem*. 1976 May 7;72:248-54.
37. Wang H, Joseph JA. Quantifying cellular oxidative stress by dichlorofluorescein assay using microplate reader. *Free Radic Biol Med*. 1999;27(5-6):612-616.
38. Wojtala A, Bonora M, Malinska D, et al. Methods to monitor ROS production by fluorescence microscopy and fluorometry. *Methods Enzymol*. 2014;542:243-62.
39. Baker MA, He S. Elaboration of cellular DNA breaks by hydroperoxides. *Free Radic Biol Med*. 1991;11(6):563-572.
40. Vistica DT, Skehan P, Scudiero D, et al. Tetrazolium-based assays for cellular viability: a critical examination of selected parameters affecting formazan production. *Cancer Res*. 1991 May 15;51(10):2515-20.
41. Zhang Y, Chen X, Gueydan C, et al. Plasma membrane changes during programmed cell deaths. *Cell Res*. 2018 Jan;28(1):9-21.
42. Wlodkowic D, Telford W, Skommer J, et al. Apoptosis and beyond: cytometry in studies of programmed cell death. *Methods Cell Biol*. 2011;103:55-98.
43. Gutteridge JMC, Halliwell B. *Free Radicals in Biology and Medicine* Oxford University Press; 2015.

44. Park J, Lee J, Choi C. Mitochondrial network determines intracellular ROS dynamics and sensitivity to oxidative stress through switching inter-mitochondrial messengers. *PLoS One*. 2011;6(8):e23211.
45. Kroemer G, Galluzzi L, Brenner C. Mitochondrial membrane permeabilization in cell death. *Physiol Rev*. 2007 Jan;87(1):99-163.

II. SIMULTANEOUS DETERMINATION OF TIOPRONIN AND ITS PRIMARY METABOLITE IN PLASMA AND OCULAR TISSUES BY HPLC

Justin Beltz¹, Annalise Pfaff¹, Nuran Ercal^{1*}

¹Department of Chemistry, Missouri University of Science and Technology, Rolla, Missouri, 65409, United States

*Corresponding Author

Address: Department of Chemistry
Missouri University of Science and Technology
400 West 11th Street
Rolla, MO 65409

E-mail: nercal@mst.edu

ABSTRACT

Tiopronin, formally 2-mercaptopropionylglycine (MPG), is currently prescribed to treat cystinuria and rheumatoid arthritis, and its antioxidant properties have led to its investigation as a treatment for cataracts, a condition in which oxidative stress is strongly implicated. To study its accumulation in the eye, a reliable, isocratic HPLC method was developed for the determination of MPG and its primary metabolite 2-mercaptopropionic acid (MPA) in plasma and relevant ocular tissues. This method utilizes pre-column derivatization and fluorescence detection. The 3.5 min separation enables high-throughput analysis, and validation experiments demonstrated that this method is suitable for evaluating ocular accumulation of MPG and MPA at concentrations as low as 66 and 33 nM, respectively. Excellent linearity was achieved over the working concentration range with $R^2 > 0.997$. Extraction recovery was reproducible within each matrix and

exceeded 97%. Accuracy was within 13.3% relative error, and intra- and inter-day precisions were within 6% CV and 7% CV, respectively. Sample stability was demonstrated under various storage conditions, and the use of an internal standard conferred exceptional ruggedness. This method has been successfully applied for the determination of MPG and MPA in plasma, cornea, lens and retina following intraperitoneal administration of the drug in Wistar rats.

1. INTRODUCTION

MPG is a small-molecular weight synthetic aminothiols. It is also known by the generic name tiopronin. It is primarily used to treat cystinuria and rheumatoid arthritis.(Carlsson, Denneberg, Emanuelsson, Kagedal, & Lindgren, 1993) Its thiol moiety confers antioxidant properties such as the ability to scavenge free radicals (Castañeda-Arriaga, Vivier-Bunge, & Raul Alvarez-Idaboy, 2016) and undergo thiol disulfide exchange.(Lindell, Denneberg, & Jeppsson, 1995) It has also been investigated as a potential treatment for cataracts, (Ichikawa et al., 1980; Jiang, Sun, Shen, Wang, & Wang, 2009) in which oxidative stress has been strongly implicated.(Lou & Dickerson, 1992; Truscott, 2005)

Although oral administration of MPG is most commonly used for cystinuria or rheumatoid arthritis patients (Carlsson et al., 1993), it is not an effective route for achieving appreciable concentrations of the drug in ocular tissues, especially the lens which lacks dedicated vasculature. Local, topical administration in the form of eye drops may allow for greater accumulation of the drug at its proposed site of action with lower

dosages and fewer side-effects, but only if sufficient concentrations can be achieved in the surrounding tissues to allow for diffusion or transport into the lens.(Järvinen, Järvinen, & Urtti, 1995) Unfortunately, rapid elimination in tear fluid and numerous anatomical barriers prevent accumulation of MPG in the lens when instilled as eye drops. Drug delivery vehicles may be able to overcome this obstacle, (Abdelkader, Alany, & Pierscionek, 2015; Jiang et al., 2009) but evaluating their efficacy for this application poses several key challenges. As shown in Figure 1, MPG is quickly metabolized to 2-mercaptopropionic acid (MPA) in plasma.(Hercelin et al., 1992)

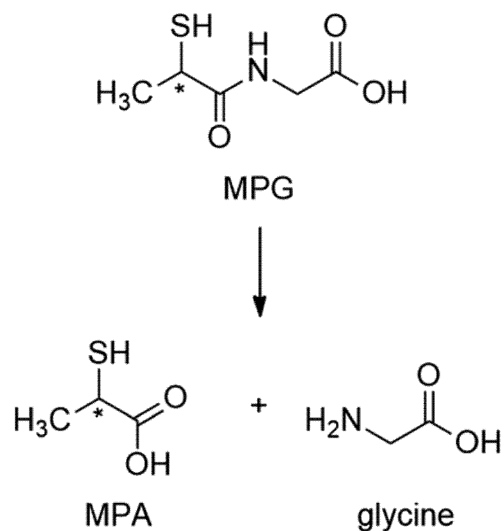


Figure 1. Hydrolysis of MPG to MPA.

In addition, preliminary experiments in our lab suggest that MPA itself is a potent antioxidant, and simply measuring ocular tissue levels of MPG alone provides an incomplete picture of its fate and distribution after administration. An ideal method

would be able to simultaneously determine levels of MPG and its major metabolite, MPA.(Hercelin et al., 1992) In addition, a highly sensitive and specific method is necessary when working with very limited sample quantities and highly complex biological matrices such as rodent cornea or retina (Dalle-Donne & Rossi, 2009).

If the method is to be used for such analyses, validation in the matrices of interest is also important. In this case, the cornea, lens, and retina are of primary interest. The cornea is the foremost obstacle to ocular drug penetration, and understanding the drug's interaction with this tissue may provide key insights for improving its ability to mediate effects in more posterior structures such as the lens.(Järvinen et al., 1995) As cataracts are the result of oxidative damage to crystallin proteins in the lens, this tissue is the proposed primary site of action for MPG. Additionally, the lens serves as an antioxidant reservoir, (Lim, Umapathy, Grey, Vaghefi, & Donaldson, 2017) and applying MPG may help to restore redox balance, thereby inhibiting processes leading to opacification. The retina is highly metabolically active and therefore sensitive to disruptions to ocular redox balance. In addition, its proximity to the ocular blood supply can provide additional information regarding influx and elimination of MPG and MPA. Finally, because a large proportion of any drug instilled in eye drop form is eliminated by tear fluid and passes into the bloodstream, (Järvinen et al., 1995) plasma levels of MPG and MPA are also of interest for understanding the ocular uptake of this drug. Finally, practical considerations such as ease of implementation and sample processing should be taken into consideration for experiments involving time-sensitive materials, such as biological tissues and drugs with labile thiol functional groups. In these cases, robust methods that offer rapid and

convenient quantification of drug concentration are preferred for high-throughput routine analyses. (McMenamin, Himmelfarb, & Nolin, 2009)

Other methods exist for determination of MPG in tissues. (Dalle-Donne & Rossi, 2009) While most methods employ HPLC separation, detection methods vary. Some rely on UV detection, which can suffer from limited sensitivity and interference in complex matrices. Others employ mass spectrometric detection, which may not be accessible or practical in many cases. Fluorescence detection, on the other hand, is both highly sensitive and economical, making it the most popular method for detection of thiol compounds. (McMenamin et al., 2009) Indeed, our group has previously demonstrated successful quantification of biologically relevant thiols, including MPG, via derivatization with maleimide dyes and HPLC separation of the fluorescent adducts. (Penugonda, Wu, Mare, & Ercal, 2004; Ridnour, Winters, Ercal, & Spitz, 1999; Wu, Goldstein, Adams, Matthews, & Ercal, 2006) However, the method described here offers several significant improvements in terms of robustness, convenience, precision, accuracy, and analysis time. It also eliminates critical matrix interferences from lens samples which were not validated in the previous technique. It entails an isocratic RP-HPLC separation following pre-column derivatization of free thiols with ThioGlo-3, a maleimide-based fluorogenic probe (see Figure 2). Prior to derivatization, reduction with tris(2-carboxyethyl)phosphine (TCEP) and addition of an internal standard minimize effects of thiol oxidation during processing. The following validation studies demonstrate that this method can accurately and reliably quantify both MPG and its major metabolite MPA in ocular tissues and plasma at nanomolar concentrations.

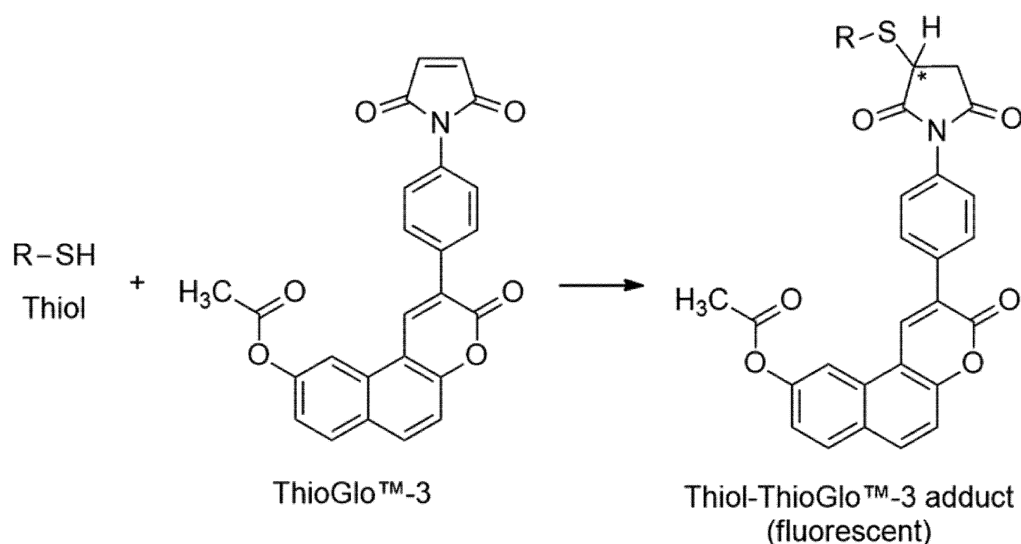


Figure 2. Derivatization of thiols with ThioGlo-3.

2. EXPERIMENTAL METHODS

2.1. CHEMICALS AND REAGENTS

MPG, MPA, N-acetylcysteine (NAC), TCEP, Tris-HCl, L-serine, and diethylenetriaminepentaacetic acid (DETAPAC) were all purchased from MilliporeSigma (St. Louis, MO, USA). Type I water was obtained using a Millipore Simplicity 185 water purification system. ThioGlo-3 was purchased from Covalent Associates, Inc. (Bellingham, WA, USA). All other reagents were purchased from Fisher Scientific (Pittsburgh, PA, USA). was adjusted to pH 7.4 with NaOH. All other reagents were purchased from Fisher Scientific. The injection vehicle for the animal study was a phosphate buffered saline (pH 7.4) consisting of 137 mM NaCl, 2.7 mM KCl, 8 mM Na₂HPO₄, and 1.5 mM KH₂PO₄. Serine borate buffer (SBB) consisting of 100 mM Tris-HCl, 5 mM L-serine, 10 mM H₃BO₃, and 1 mM DETAPAC was prepared in type 1 water and adjusted to pH 7.0 with NaOH.

2.2. ANIMALS

All animal procedures were approved by the Missouri University of Science and Technology Animal Care and Use Committee. A litter of male Wistar rats weighing 12-18 g were purchased from Charles River Laboratories (Wilmington, MA, USA). All animals were housed in a temperature-controlled room with a 12 h light-dark cycle. The rats were fed and watered *ad libitum* with Purina rat chow and municipal tap water. Six rats were fasted overnight prior to receiving an intraperitoneal injection of either MPG (250 mg/kg body weight) or vehicle alone. Forty minutes after receiving the injection, the animals were anesthetized, and blood was collected into heparin-coated Vacutainers (BD, Franklin Lakes, NJ, USA) via intracardiac puncture. The animals were euthanized and the whole eyes were immediately removed and carefully dissected in isotonic PBS to obtain the corneas, lenses, and retinas. Plasma was collected after centrifugation of whole blood samples at $2000 \times g$. All samples were stored in a freezer at -80°C until analysis.

2.3. SAMPLE PREPARATION

Corneas, lenses, and retinas were thawed and transferred to microcentrifuge tubes containing 500 μL of ice-cold SBB, spiked with 2.5 μM internal standard (NAC) and 75 μM TCEP. The tissues were sheared in this buffer on ice using a Tissue-Tearor (BioSpec Products, Inc., Bartlesville, OK, USA). The samples were removed from ice and allowed to stand for 30 min for temperature equilibration and reduction of disulfide bonds. Matrix protein content was determined via the Coomassie dye-binding method described by Bradford. (Bradford, 1976) Briefly, Bradford dye reagent (Bio-Rad, Hercules, CA, USA) was diluted five-fold in SBB, and 2.5 μL of the working reagent was added to 50 μL of

tissue homogenate. The absorbance at 595 nm was recorded after 5 min. Aliquots from lens and retina homogenates were diluted 15-fold and 2-fold, respectively to keep protein levels within the working linear range for the Bradford assay. The homogenates were then centrifuged for 5 min at $11,000 \times g$. For derivatization, 100 μL of the supernatant solutions were transferred to tubes containing 25 μL of SBB and 375 μL of ThioGlo-3 (33 μM in HPLC-grade acetonitrile). After 20 min, samples were acidified with 5 μL of 2 N HCl, and then diluted with 250 μL of mobile phase component A.

Plasma samples were thawed, and 40- μL aliquots of plasma were diluted with 160 μL of SBB spiked with 2.5 μM internal standard and 75 μM TCEP, and allowed to stand for 30 min. The diluted plasma samples were then centrifuged for 5 min. at $11,000 \times g$. Then, 125 μL of the supernatant solutions were transferred to tubes containing 375 μL of 33- μM ThioGlo-3. After 20 min, samples were acidified with 5 μL of 2 N HCl, and then diluted with 250 μL of mobile phase component A.

The samples were filtered into sampler vials using 0.2- μm nylon syringe filters (Fisher Scientific).

2.4. PREPARATION OF CALIBRATION STANDARDS

Calibration standards were prepared by spiking 25 μL of working solutions of MPG and MPA into 100 μL of pooled drug-free samples of the corresponding matrix, diluted in SBB spiked with internal standard and TCEP. The final concentrations of NAC and TCEP all of the calibration standards were 331 nM and 9.93 μM , respectively.

Calibration standards were prepared at 9 levels over the range of 66.2 – 1656 nM for MPG and 33.1 – 828 nM for MPA.

2.5. HPLC PARAMETERS

A Thermo Scientific Dionex UltiMate 3000 Series HPLC system equipped with a Dionex LPG-3400-SD pump, a Dionex ACC-3000 autosampler, and a Dionex FLD-3100 fluorescence detector was used for the duration of this study. The analytes were separated in a Kinetex C₁₈ column (75 mm × 4.6 mm i.d.) with 2.6-μm superficially porous particles (Phenomenex, Torrance, CA, USA). The column oven was set to 30°C. The mobile phase was prepared by on-line mixing of two components (isocratic 1:1 blend). Component A was prepared by diluting 1.00 mL of 85% H₃PO₄ (HPLC-grade) to 900 mL with Type 1 water, adjusting the pH to 2.46 by dropwise addition of NaOH, and diluting to a final volume of 1 L. Component B was prepared by mixing 200 mL of component A with 800 mL of HPLC-grade acetonitrile. Both components were filtered using 0.22-μm nylon membrane filters (Foxy Life Sciences, Salem, NH, USA) and degassed prior to use. The mobile phase was pumped at a flow rate of 3.0 mL/min. Separation was completed within 3.5 min. The xenon lamp was operated in “Standard” mode, and the detector sensitivity settings were adjusted according to the timetable shown in Table 1.

Table 1. Detector settings

Time, min	Excitation λ, nm	Emission λ, nm	Sensitivity level*
0.000	365	445	1
0.760	365	445	5
1.900	365	445	8

*Each sensitivity level represents an 8-fold increase in detector response.

2.6. METHOD VALIDATION

Validation of the method described here was performed in accordance with the USP and ICH guidelines. Specific definitions and approaches to the parameters validated are given below:

2.6.1. Selectivity. Selectivity was determined for each matrix. Spiked and unspiked samples of each matrix taken from six different animals were individually processed and analyzed as described above. Chromatograms from spiked and unspiked samples were compared to determine whether there were any endogenous sources of interference with the NAC, MPG, and MPA peaks.

2.6.2. Linearity and LLOQ. Linearity was assessed from calibration standards prepared at nine concentration levels for each matrix. Standards for each calibration point were prepared in triplicate. Concentration ranges were chosen to reflect those expected after administration of MPG. For each curve, the concentration of calibration standards was plotted against the analyte's peak area relative to that of the internal standard. Calibration curves were calculated by unweighted linear least-squares regression. The LLOQ in each matrix was accepted as the lowest standard concentration point on the curve that exhibited less than 20% RSD from the mean and less than 20% relative deviation from the target concentration.

2.6.3. Sample Stability. The stability of the processed samples was evaluated for typical storage conditions, including storage on the autosampler tray at 30°C for up to 12 hours, at 4°C for up to one week, and after three freeze-thaw cycles from -80°C. Stability of MPG and MPA in sample matrix was also evaluated over 3 hours at room temperature and 48 hours at -80°C. The determination of sample stability was made using triplicate

samples matrices spiked with low (166 nM MPG, 83 nM MPA) and high (662 nM MPG, 331 nM MPA) levels of MPG and MPA. Stability was reported as the ratio of the detector response obtained from samples subjected to the indicated storage conditions to that of replicate samples injected immediately.

2.6.4. Precision, Accuracy, and Recovery. Precision, accuracy, and relative recovery were evaluated in each matrix spiked with high (662 nM MPG, 331 nM MPA), medium (331 nM MPG, 166 nM MPA), and low (166 nM MPG, 83 nM MPA) levels of MPG and MPA. Five replicate samples were analyzed for each level. Intra-assay precision is reported as the coefficient of variation (%CV) of five replicate samples analyzed in the same analytical run. Inter-assay precision is reported as the %CV for 15 replicate spiked samples processed over three different days by two different analysts with freshly prepared reagents. For determination of relative recovery, spiking solutions of MPG and MPA were added to samples prior to sample processing. The recovery is reported as the ratio of the detector response from samples spiked before processing to the response obtained from analogous samples spiked just prior to derivatization.

3. RESULTS AND DISCUSSION

MPG is an important pharmaceutical for the management of diseases such as cystinuria and rheumatoid arthritis, and its antioxidant properties may find use in a number of oxidative stress-related conditions, including cataracts and other age-related eye diseases. For this purpose, it is necessary to understand the distribution of MPG and its major metabolite MPA in ocular tissues as well as its absorption into the bloodstream.

Moreover, preliminary experiments conducted in our lab suggest that MPA is also a potent free radical scavenger, and as such, an important contributor to the therapeutic effects of MPG. In recent years, drug delivery vehicles have emerged as a promising strategy for increasing drug penetration and residence in the eye. However, in order to evaluate their ability to increase MPG concentrations in the eye, a sensitive and reliable method for monitoring MPG levels in ocular tissues needed to be developed and validated.

3.1. CHROMATOGRAPHY

The method described herein is based on one previously developed by our group (Penugonda et al., 2004). However, the newer method offers several key advantages over the original and overcomes some key limitations. Although the method described by Penugonda *et al.* was suitable for determination of MPG in a number of other biological matrices, it was not suitable for our more recent studies investigating ocular drug uptake. This was mainly due to the presence of endogenous compounds that would co-elute with MPG. As a result, it was necessary to modify and re-validate the method for this application. In order to achieve the separation required to eliminate the interference, a column with higher efficiency was selected, and a new mobile phase composition was optimized based on the results of typical scouting gradient experiments.

Some representative chromatograms are shown in Figure 3. ThioGlo-3 alone produced a detectable peak at 3.4 min. Addition of TCEP gave rise to a high intensity peak that is retained for 0.5 min, and a lower intensity peak with a retention time of 1.7 min. The internal standard, NAC, is retained for 1.1 min. Derivatization of MPG and

MPA gave rise to two peaks each. Derivatized adducts of MPG were eluted after 1.3 min and 1.4 min, and adducts of MPA were eluted after 2.3 min and 2.5 min.

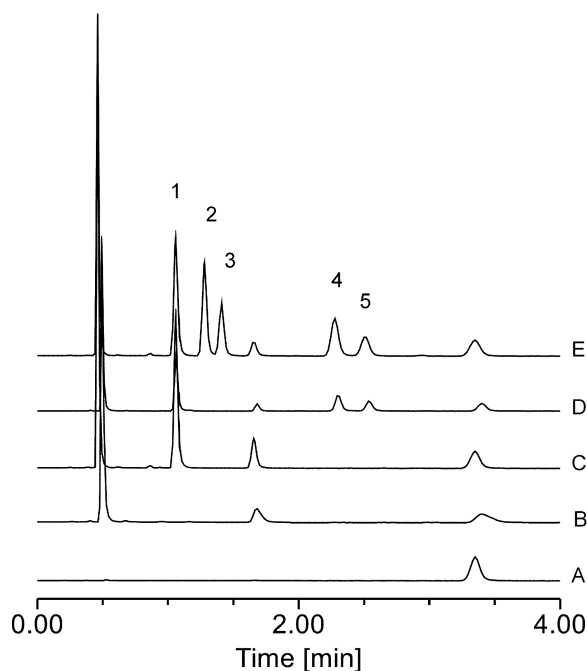


Figure 3. Overlay of representative chromatograms from samples containing A, ThioGlo-3 in sample diluent; B, ThioGlo-3 + TCEP; C, ThioGlo-3 + TCEP + NAC; D, ThioGlo-3 + TCEP + NAC + MPA; E, ThioGlo-3 + TCEP + NAC + MPG + MPA. The peaks are associated with the indicated analytes 1, NAC; 2,3, MPG; 4,5, MPA.

MPG and MPA are both chiral thiols, each containing a single stereocenter. When these chiral thiols react with a maleimide probe such as ThioGlo-3, a second stereocenter is formed as shown in Figure 4. Thus, four stereoisomers are possible. (Kullman et al., 2000) We hypothesize, therefore, that the two diastereomeric pairs were separated due to the increased chromatographic efficiency of this method. Although multiple products were formed following derivatization of MPG and MPA, quantitation was not significantly hindered. The formation of fluorescent adducts following derivatization with

ThioGlo-3 was quantitative and reproducible, and the results were consistent when using MPG sourced from different manufacturing lots. Furthermore, baseline resolution was achieved for all relevant peaks across the working concentration range (resolution > 2.07, USP). For determination of MPG and MPA, the greatest precision and accuracy were achieved by integrating the peaks eluting at 1.4 min for MPG and 2.3 min for MPA.

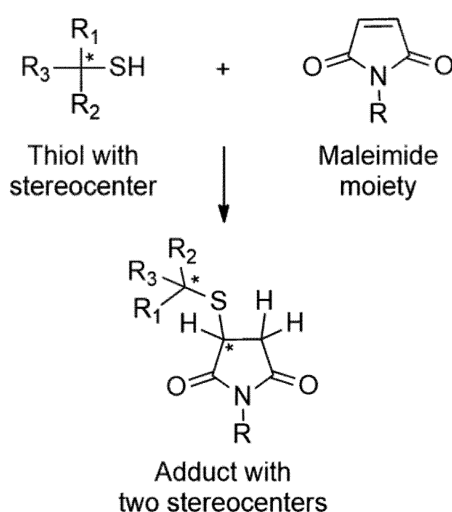


Figure 4. Derivatization of thiols containing a stereocenter gives rise to products with two stereocenters.

As an isocratic separation that is completed within 3.5 min, this method requires only 12 mL of mobile phase per run, only 40% of which is organic solvent. Furthermore, this method offers greater sensitivity than those utilizing UV detection and poses less of an economic barrier to researchers compared to methods utilizing LC-MS, which can be prohibitively expensive to acquire and maintain. Thus, the method described here is faster, more economical, and more environmentally friendly than many existing techniques.

3.2. SELECTIVITY

Figure 5 shows representative chromatograms obtained from the analysis of spiked and unspiked plasma, cornea, lens, and retina extracts. The matrices investigated did not contain any detectable, endogenous compounds that would co-elute and interfere with the analytes of interest. Most of the endogenous aminothiols such as GSH, cysteine, homocysteine, and CysGly elute within the first 60 seconds. The derivatization technique coupled with the separation and detection method produces interference-free chromatograms, making the technique selective for NAC, MPG and MPA.

3.3. LINEARITY AND LLOQ

The calibration curves (sample shown Figure 6) were created by plotting the concentration of calibration standards vs. the analyte's peak area relative to that of the internal standard. The regression data from each calibration curve is summarized in Table 2. The linear ranges achieved for MPG and MPA in each of the matrices were suitable for determinations in real samples. The smallest level on the calibration curve that was accurate within 20% of the target concentration and with less than 20%RSD was accepted as the LLOQ for MPG and MPA in each matrix. The LLOQs achieved ranged from 66 – 99 nM for MPG and were < 33 nM for MPA per 10 μ L injection. Given the drug availability challenges associated with the eye and the relatively small size of the ocular tissues, low LLOQs are necessary for studies investigating ocular drug uptake and retention. This is difficult to achieve with other methods available such as those utilizing UV detection; however, the use of fluorescence detection offers much higher sensitivity. (Kusmierek, Chwatko, Glowacki, & Bald, 2009) One disadvantage resulting

from the separation of stereoisomers of MPG and MPA is that the LOD and LLOQ are increased; however, the limits were still suitable for our applications.

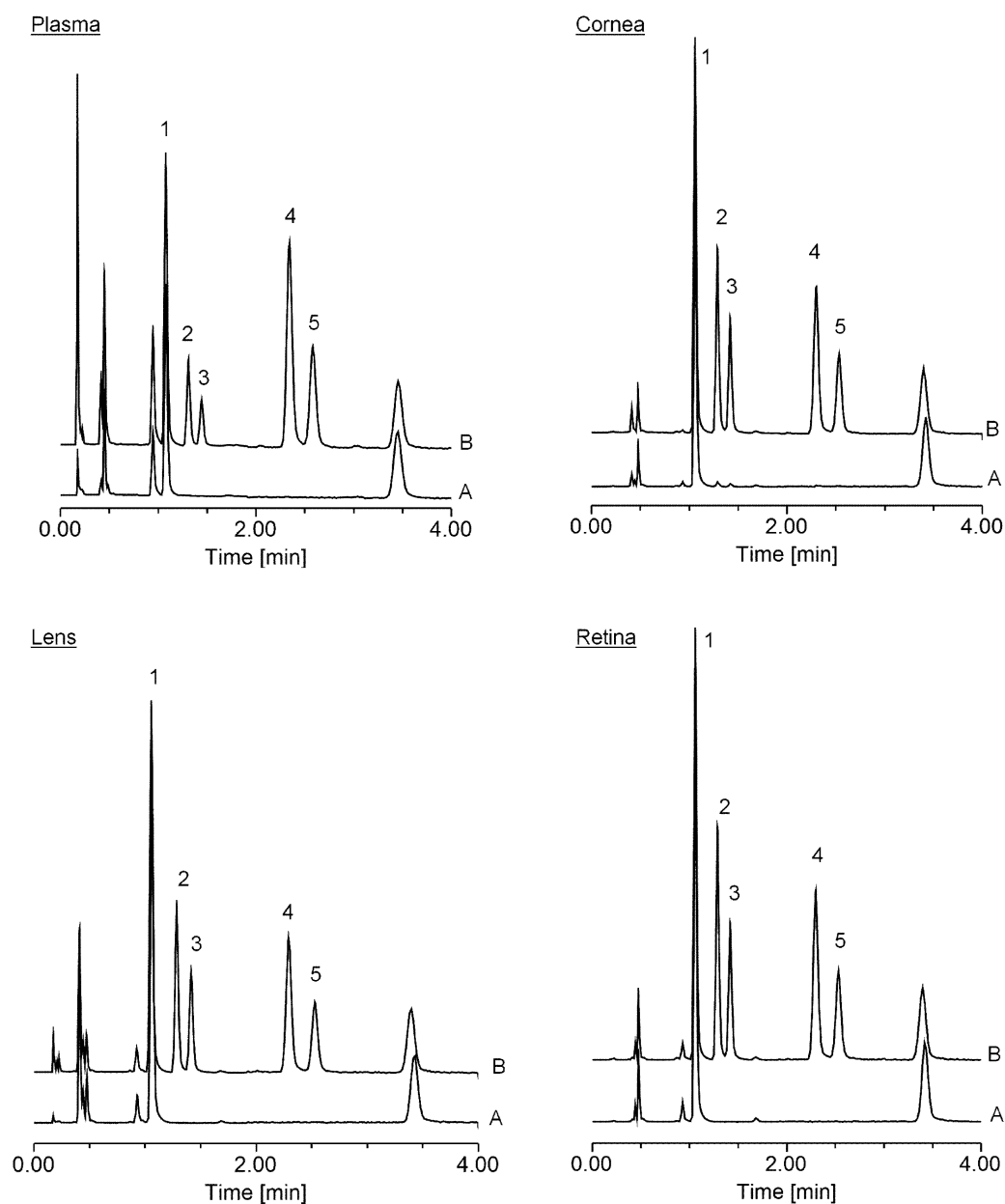


Figure 5. Representative chromatograms from processed tissue samples. Each plot depicts an overlay of the spiked matrix (B) on top of the unspiked matrix (A). Spiked matrices contained 500 pmol of NAC, 500 pmol of MPG, and 250 pmol of MPA during derivatization. Unspiked matrices contained 500 pmol of NAC. Peak labels: 1, NAC ; 2,3, peaks arising from MPG derivatization; 4,5, peaks arising from MPA derivatization.

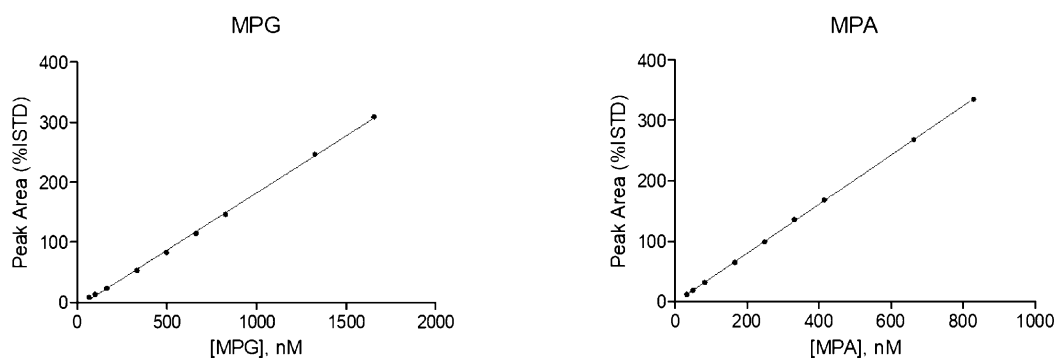


Figure 6. Calibration curves for MPG (left) and MPA (right) diluted in SBB. The solid black dots represent the mean response from three replicate injections.

Table 2. Summary of linear regression

Matrix	Analyte	Regression equation	R ²	Linear range, nM	LLOQ, nM ^a
SBB	MPG	$y = 0.1904x - 8.319$	0.9991	66 - 1656	99.34
	MPA	$y = 0.4078x - 1.616$	0.9997	33 - 828	33.11
Plasma	MPG	$y = 0.0566x - 2.9861$	0.9979	66 - 828	66.23
	MPA	$y = 0.778x - 6.1789$	0.9998	33 - 828	33.11
Cornea	MPG	$y = 0.1958x - 12.1028$	0.9987	66 - 1656	66.23
	MPA	$y = 0.442x - 3.085$	0.9998	33 - 828	33.11
Lens	MPG	$y = 0.2363x - 11.5415$	0.9997	66 - 1656	66.23
	MPA	$y = 0.738x - 6.9977$	0.9997	33 - 828	33.11
Retina	MPG	$y = 0.2171x - 15.8672$	0.9973	66 - 1656	99.34
	MPA	$y = 0.4418x - 2.9531$	0.9999	33 - 828	33.11

^aLLOQ is given for an injection volume of 10 μ L.

3.4. SAMPLE STABILITY

Due to the oxidizable nature of the aminothiols and the nature of the sample, it is important to ensure that the sample will be stable enough under typical storage and exposure conditions to be reliably analyzed. Since aminothiols are prone to oxidation, it is recommended to derivatize or otherwise stabilize the samples as soon as possible. Spiked matrix samples left at room temperature for 3 hours or frozen at -80°C

for 48 hours before reduction and derivatization provided results within 2% deviation from samples injected immediately. Processed samples were evaluated at 30°C for up to 12 hours to ensure stability while queued on the autosampler rack. Additionally, stability was evaluated after storage for 1 week at 4°C, as well as after three freeze-thaw cycles. The results of these experiments are summarized in Table 3. After the samples have been processed, they are stable beyond typical handling conditions. All samples were stable at 30°C for at least 12 hours. Acceptable stability was also achieved after storage for up to one week at 4°C, and after three freeze-thaw cycles of samples stored at -80°C.

Table 3. Stability of derivatized samples

Spike Level ^a		30°C		30°C		4°C		Three freeze-thaw cycles	
		6 hours		12 hours		1 week		MPG	MPA
		MPG	MPA	MPG	MPA	MPG	MPA		
SBB	L	101.9%	97.2%	99.6%	96.9%	96.2%	103.7%	95.9%	98.3%
	H	98.6%	98.2%	98.9%	96.2%	99.4%	105.7%	96.1%	93.6%
Plasma	L	96.3%	103.9%	97.6%	99.2%	97.6%	112.2%	97.6%	105.7%
	H	99.9%	98.3%	103.2%	95.3%	100.4%	100.0%	100.5%	96.8%
Cornea	L	99.5%	97.8%	101.7%	93.8%	100.6%	101.5%	99.2%	98.3%
	H	100.0%	100.5%	100.8%	99.8%	99.0%	99.6%	98.9%	96.3%
Lens	L	98.0%	98.0%	98.3%	95.7%	97.8%	104.2%	97.7%	103.5%
	H	99.3%	97.2%	99.4%	95.0%	99.1%	103.1%	97.7%	99.8%
Retina	L	100.0%	100.9%	99.1%	99.8%	97.3%	110.2%	98.1%	111.9%
	H	101.0%	100.3%	101.8%	97.9%	97.0%	100.0%	97.7%	100.7%

^a Spike levels: L, 166 nM MPG, 83 nM MPA; H, 662 nM MPG, 331 nM MPA

The convenient one-step reduction and addition of internal standard provides for greater sample stability with respect to oxidation, evaporation, and processing.

Furthermore, the reduction step allows for determination of *total* MPG and MPA, by freeing up protein bound MPG and MPA or other mixed disulfides. This is particularly important, as their hypothesized mechanisms of action involve thiol-disulfide exchange, indicating that a significant portion of MPG and MPA may be oxidized at their sites of action.

3.5. PRECISION, ACCURACY, AND RECOVERY

Precision, accuracy, and relative recovery were determined according to the USP and ICH guidelines. The results are summarized in Table 4.

Table 4. Precision, accuracy, and recovery

Matrix	Spike Level ^a	Precision				Accuracy		Relative Recovery	
		Intra-day (%CV)		Inter-day (%CV)		(%RE)		(% , mean \pm S.D.)	
		MPG	MPA	MPG	MPA	MPG	MPA	MPG	MPA
SBB	L	0.51	1.11	3.00	2.16	10.14	-3.85	n.a.	n.a.
	M	0.34	1.38	2.28	2.23	1.99	-3.72	n.a.	n.a.
	H	0.16	0.52	0.56	1.07	0.74	-1.13	n.a.	n.a.
Plasma	L	4.15	3.03	6.99	3.65	-10.25	5.16	111.3 \pm 2.39	97.4 \pm 2.36
	M	5.40	0.76	5.89	2.83	-8.74	1.50	104.5 \pm 4.43	98.8 \pm 1.56
	H	2.59	1.29	2.72	2.32	-13.25	-1.19	111.4 \pm 8.07	102.4 \pm 1.13
Cornea	L	0.65	0.98	3.40	1.32	-3.06	-2.49	98.3 \pm 0.14	100.1 \pm 1.71
	M	0.29	0.55	2.09	1.68	5.42	-4.14	96.4 \pm 0.59	102.3 \pm 0.61
	H	0.10	0.30	0.78	0.67	5.66	-4.26	99.9 \pm 1.60	102.0 \pm 0.38
Lens	L	2.04	2.17	4.50	2.67	-4.63	5.45	110.9 \pm 2.96	99.1 \pm 4.08
	M	0.60	1.01	3.61	1.48	-7.31	0.98	111.7 \pm 0.53	102.5 \pm 1.50
	H	0.60	0.69	1.23	0.75	-5.02	1.77	111.3 \pm 0.72	102.5 \pm 1.97
Retina	L	0.84	1.95	1.01	2.28	4.11	-3.34	99.4 \pm 0.45	104.5 \pm 0.34
	M	0.21	0.67	1.96	2.25	0.43	-2.76	99.5 \pm 1.43	103.3 \pm 0.50
	H	0.26	0.30	1.16	1.04	1.26	-4.79	101.4 \pm 1.92	105.0 \pm 0.36

^a Spike levels: L, 166 nM MPG, 83 nM MPA; M, 331 nM MPG, 166 nM MPA; H, 662 nM MPG, 331 nM MPA

Intra-day and inter-day precision for all samples were below 5.5% and 7.0% RSD, respectively. Determinations in plasma samples were accurate within 13.3% of the spiked concentration while those from ocular tissues were accurate within 7.4% of the spiked concentration. The relative recovery was consistent across low, medium, and high spikes of MPG and MPA within matrices. All values were within the acceptability criteria.

3.6. DETERMINATION OF MPG AND MPA IN PLASMA AND OCULAR TISSUES

The method validated as described above was successfully applied for the simultaneous determination of MPG and MPA in Wistar rat plasma and ocular tissues following injection of MPG. Wistar rats were administered PBS or MPG (250 mg/kg body weight) by intraperitoneal injection. This dose is relatively high compared to those used in human patients, which was necessary in order to observe even low levels of MPG in ocular tissues. None of the animals were given MPA. Samples were processed as described in the methods section. The results are summarized in Table 5.

Table 5. MPG and MPA concentration in Wistar rat tissues 40 min after intraperitoneal administration of MPG

Sample	[MPG]	[MPA]
	Mean \pm Standard Deviation (N = 3)	
Plasma	88.30 \pm 9.13 μ M	9.13 \pm 3.50 μ M
Cornea	11.93 \pm 1.36 nmol/mg protein	1.36 \pm 1.06 nmol/mg protein
Lens	0.41 \pm 0.12 nmol/mg protein	0.12 \pm 0.07 nmol/mg protein
Retina	2.43 \pm 1.42 nmol/mg protein	Not detected

No MPG or MPA was detected in samples collected from animals injected with PBS. Both MPG and MPA were present in plasma, cornea, and lens samples from the animals that were injected with MPG. Since MPA was not detected in the animals injected with PBS, this indicates that MPG was metabolized to MPA following injection. The retina did not contain detectable levels of MPA, but low levels of MPG were present.

Although a similar method for analysis of MPG in biological tissues was developed in our lab and described by Penugonda (Penugonda et al., 2004), endogenous interferences prevented determination of MPG in lens tissue, and thus it was unsuitable for evaluating ocular uptake of MPG. Furthermore, the method described here offers a number of significant improvements over the previous method: First of all, this method simultaneously measures concentrations of MPA as well as MPG. In addition, TCEP reduction allows for determination of total MPG, comprising its oxidized and reduced forms. The current method's use of an internal standard greatly improves accuracy and robustness. Finally, the new method is twice as fast. Therefore, this method is more suitable for evaluating drug delivery vehicles designed to enhance the ocular uptake of MPG.

4. CONCLUSION

A reliable HPLC-FLD method was developed for simultaneous determination of MPG and its major metabolite, MPA. Because this drug exhibits potential as an antioxidant treatment for cataracts, the method was validated in ocular tissue matrices and plasma for the purpose of monitoring the uptake and distribution of the drug

throughout treatment. The method was successfully applied to the analysis of plasma and ocular tissues of animals injected with MPG, wherein both analytes MPG and MPA were detected in animals treated with the drug. While other techniques for the analysis of MPG exist, the method described here accomplishes it isocratically in under 4 minutes with widely available instrumentation. Moreover, the reduction step and internal standard confer stability with respect to oxidation during processing and other variations in sample handling, making this method ideal for routine analysis of MPG and MPA in both basic research and clinical settings.

ACKNOWLEDGMENTS

This research was made possible by the Richard K. Vitek/FCR Endowment.

REFERENCES

- Abdelkader, H., Alany, R. G., & Pierscionek, B. (2015). Age-related cataract and drug therapy: opportunities and challenges for topical antioxidant delivery to the lens. *J Pharm Pharmacol*, 67(4), 537-550. doi:10.1111/jphp.12355
- Bradford, M. M. (1976). A rapid and sensitive method for the quantitation of microgram quantities of protein utilizing the principle of protein-dye binding. *Anal Biochem*, 72, 248-254.
- Carlsson, M. S., Denneberg, T., Emanuelsson, B. M., Kagedal, B., & Lindgren, S. (1993). Pharmacokinetics of oral tiopronin. *European Journal of Clinical Pharmacology*, 45(1), 79-84. doi:10.1007/bf00315354
- Castañeda-Arriaga, R., Vivier-Bunge, A., & Raul Alvarez-Idaboy, J. (2016). Primary antioxidant and metal-binding effects of tiopronin: A theoretical investigation of its action mechanism. *Computational and Theoretical Chemistry*, 1077, 48-57. doi:10.1016/j.comptc.2015.10.012

- Dalle-Donne, I., & Rossi, R. (2009). Analysis of thiols. *Journal of Chromatography. B: Analytical Technologies in the Biomedical and Life Sciences*, 877(28), 3271-3273. doi:10.1016/j.jchromb.2009.08.034
- Hercelin, B., Leroy, P., Nicolas, A., Gavriloff, C., Chassard, D., Thebault, J. J., . . . Netter, P. (1992). The pharmacokinetics of tiopronin and its principal metabolite (2-mercaptopropionic acid) after oral administration to healthy volunteers. *Eur J Clin Pharmacol*, 43(1), 93-95.
- Ichikawa, H., Imaizumi, K., Tazawa, Y., Obara, Y., Ishikawa, Y., Tobari, I., & Tanabe, Y. (1980). Effect of tiopronin on senile cataracts. A double-blind clinical study. *Ophthalmologica*, 180(5), 293-298.
- Järvinen, K., Järvinen, T., & Urtti, A. (1995). Ocular absorption following topical delivery. *Advanced Drug Delivery Reviews*, 16(1), 3-19. doi:10.1016/0169-409x(95)00010-5
- Jiang, T.-Y., Sun, C.-S., Shen, X., Wang, T.-Y., & Wang, S.-L. (2009). Development of a poloxamer analogs/bioadhesive polymers-based in situ gelling ophthalmic delivery system for tiopronin. *J Appl Polym Sci*, 114(2), 775-783. doi:10.1002/app.30520
- Kullman, J. P., Yu, T., Chen, X., Neal, R., Ercal, N., & Armstrong, D. W. (2000). Resolution of Chiral Thiol Compounds Derivatized with N-(1-Pyrenyl)-Maleimide and ThiogloTM3. *Journal of Liquid Chromatography & Related Technologies*, 23(13), 1941-1952. doi:10.1081/jlc-100100463
- Kusmieriek, K., Chwatko, G., Glowacki, R., & Bald, E. (2009). Determination of endogenous thiols and thiol drugs in urine by HPLC with ultraviolet detection. *Journal of Chromatography. B: Analytical Technologies in the Biomedical and Life Sciences*, 877(28), 3300-3308. doi:10.1016/j.jchromb.2009.03.038
- Lim, J. C., Umopathy, A., Grey, A. C., Vaghefi, E., & Donaldson, P. J. (2017). Novel roles for the lens in preserving overall ocular health. *Exp Eye Res*, 156, 117-123. doi:10.1016/j.exer.2016.05.027
- Lindell, A., Denneberg, T., & Jeppsson, J. O. (1995). Urinary excretion of free cystine and the tiopronin-cysteine-mixed disulfide during long term tiopronin treatment of cystinuria. *Nephron*, 71(3), 328-342. doi:10.1159/000188740
- Lou, M. F., & Dickerson, J. E. (1992). Protein-thiol mixed disulfides in human lens. *Experimental Eye Research*, 55(6), 889-896. doi:10.1016/0014-4835(92)90015-k

- McMenamin, M. E., Himmelfarb, J., & Nolin, T. D. (2009). Simultaneous analysis of multiple aminothiols in human plasma by high performance liquid chromatography with fluorescence detection. *J Chromatogr B Analyt Technol Biomed Life Sci*, 877(28), 3274-3281. doi:10.1016/j.jchromb.2009.05.046
- Penugonda, S., Wu, W., Mare, S., & Ercal, N. (2004). Liquid chromatography analysis of N-(2-mercaptopropionyl)-glycine in biological samples by ThioGlo 3 derivatization. *J Chromatogr B Analyt Technol Biomed Life Sci*, 807(2), 251-256. doi:10.1016/j.jchromb.2004.04.019
- Ridnour, L. A., Winters, R. A., Ercal, N., & Spitz, D. R. (1999). Measurement of glutathione, glutathione disulfide, and other thiols in mammalian cell and tissue homogenates using high-performance liquid chromatography separation of N-(1-pyrenyl)maleimide derivatives *Methods in Enzymology* (Vol. 299, pp. 258-267): Academic Press.
- Truscott, R. J. (2005). Age-related nuclear cataract-oxidation is the key. *Exp Eye Res*, 80(5), 709-725. doi:10.1016/j.exer.2004.12.007
- Wu, W., Goldstein, G., Adams, C., Matthews, R. H., & Ercal, N. (2006). Separation and quantification of N-acetyl-l-cysteine and N-acetyl-cysteine-amide by HPLC with fluorescence detection. *Biomed Chromatogr*, 20(5), 415-422. doi:10.1002/bmc.583

III. EFFECT OF NANODIAMOND SURFACE CHEMISTRY ON ADSORPTION AND RELEASE OF TIOPRONIN

Justin Beltz,¹ Annalise Pfaff,¹ Ibrahim Munkaila Abdullahi,¹ Alex Cristea,¹ Vadym N. Mochalin,^{1,2*} Nuran Ercal^{1**}

¹ Department of Chemistry, Missouri University of Science & Technology, 400 W. 11th Street, 104 Schrenk Hall, Rolla, MO 65409, USA

² Department of Materials Science & Engineering, Missouri University of Science & Technology, MO 65409, USA

* corresponding author e-mail: mochalinv@mst.edu

** corresponding author e-mail: nercal@mst.edu

ABSTRACT

Tiopronin is an FDA-approved thiol drug currently used to treat cystinuria and rheumatoid arthritis. However, due to its antioxidant properties, it may be beneficial in a variety of other conditions. One primary obstacle to its wider application is its limited bioavailability, which necessitates administration of high systemic doses to achieve localized therapeutic effects. Incorporation of a drug delivery vehicle can solve this dilemma by providing a means of controlled, targeted release. Functionalized nanodiamond is a promising theranostic platform that has demonstrated great potential for biomedical applications, including drug delivery. Design of nanodiamond theranostic platforms requires comprehensive understanding of drug-platform interactions, and the necessary physical chemical investigations have only been realized for a limited number of compounds. Towards the long-term goal of developing a nanodiamond-tiopronin treatment paradigm, this study aims to shed light on the effects of nanodiamond surface

chemistry on adsorption and release of tiopronin. Specifically, adsorption isotherms were measured and fit to Langmuir and Freundlich models for carboxylated, hydroxylated, and aminated nanodiamonds, and release was monitored in solutions at pH 4.0, 5.8, 7.3, and 8.1. Our results indicate that aminated nanodiamonds exhibit the highest loading capacity while hydroxylated nanodiamonds are the most effective for sustained release. Therefore, a high degree of flexibility may be afforded by the use of nanodiamonds with different surface chemistries optimized for specific applications.

Keywords: Nanodiamond; Functionalization; Adsorption; Desorption; Drug delivery

1. INTRODUCTION

Tiopronin is a low-molecular-weight thiol drug used for the treatment of rheumatoid arthritis and cystinuria. It has also demonstrated potential benefits in a variety of other conditions, including heavy metal¹ and radiation poisoning,² and cataract.³ A primary mechanism of its action in these conditions is the direct scavenging of free radicals and maintenance of healthy levels of glutathione (GSH), a vital antioxidant and the body's most abundant non-protein thiol.⁴⁻⁵ However, the effectiveness of tiopronin is limited by its bioavailability. Tiopronin is weakly acidic and becomes deprotonated at physiological pH. The negatively charged conjugate base (Figure 1) cannot easily penetrate the low polarity lipid bilayer of cell membranes. Furthermore, when administered topically, insufficient residence time on physiological barriers such as the skin or cornea can severely curtail its uptake and deeper penetration into tissues.⁶ These effects necessitate the administration of higher dosages, increasing the risk and severity

of adverse side effects. It is therefore desirable to provide a means by which small hydrophilic molecules such as tiopronin can be transported and released in a controlled manner at their desired site of action. Towards this end, drug delivery vehicles offer a promising alternative to the large systemic doses of neat drug and excipient used currently.⁷ For example, it has been shown that poloxamer hydrogels significantly enhanced uptake and effectiveness of tiopronin in a rat model of age-related nuclear cataracts.⁸

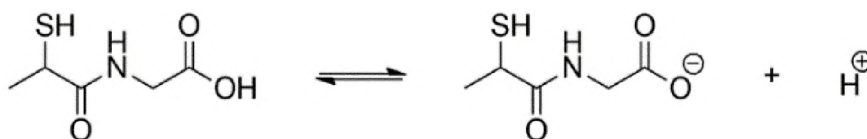


Figure 1. Tiopronin microspecies in equilibrium.

In addition to providing controlled transport and release of a well-defined and therapeutically consequential payload, drug delivery vehicles must be highly biocompatible and stable under formulation conditions (which may include autoclaving or irradiation). Sustained release is also desirable, given that the conditions mentioned above may be long-term or chronic illnesses. In these respects, hydrogels present many challenges with regard to chemical stability, longevity, and especially sustained and controlled release.⁹ Nanodiamonds (NDs), however, are not subject to these limitations. Detonation nanodiamonds, which are inexpensive and commercially available, are nontoxic and are considered the most biocompatible of all carbon nanoparticles.¹⁰ Each ND particle possesses a core of sp^3 hybridized carbon that is chemically inert and similar to bulk diamond, while the surface comprises fully exposed, covalently attached

functional groups that can be tailored for optimal interaction with the drug payload and environment.¹⁰⁻¹¹ Modification of surface chemistry affords a high degree of control, specificity, and flexibility with respect to drug-ND interaction.¹²⁻¹⁴ Here we investigate the potential of ND as a promising candidate platform for delivery and sustained release of tiopronin.

A critical step in assessing the suitability of a drug delivery platform is to determine its capacity to carry and release the compound of interest.

Adsorption/desorption is the simplest and therefore preferred mechanism of loading and release. It requires no chemical modification of the drug, which reduces risks of interfering with its biological activity.¹³ The rich surface chemistry of ND allows for a high degree of control over drug-ND interactions, which is exerted through the creation of functional groups such as -COOH, -OH, or -NH₂ on the ND surface. Controlling ND surface chemistry can significantly affect loading capacity, strength of binding, and release of the desired drug.¹⁴ Because tiopronin is negatively charged at physiological pH, the electrostatic interaction between adsorbent and adsorbate can be tailored to optimize the drug delivery platform.

Although understanding adsorption and release is essential for development of ND-drug complexes capable of delivering well-defined dosages, these phenomena have been largely unexplored for ND as a carrier of tiopronin or other similar thiol drugs. By understanding the effects of surface functionalization on ζ -potential, adsorption monolayer capacity, and cumulative drug release, we can determine the optimal surface chemistry for ND-mediated delivery of tiopronin for a variety of conditions. Consistent and reliable delivery of tiopronin and related compounds can pave the way for more

targeted treatment regimens that produce the same therapeutic effects with significantly lower incidence of side effects.

2. EXPERIMENTAL METHODS

2.1. MATERIALS AND REAGENTS

UD90 ND powder was donated by NanoBlox, Inc. Tiopronin, tris(2-carboxyethyl)phosphine (TCEP), N-acetylcysteine (NAC), and K_2HPO_4 were purchased from MilliporeSigma (St. Louis, MO, USA). ThioGlo-3 was purchased from Covalent Associates Inc. (Bellingham, WA, USA). All other reagents were purchased from Fisher Scientific (Pittsburgh, PA, USA). Type 1 water was prepared in-house using a Millipore Simplicity 185 purification system (MilliporeSigma). Citrate-phosphate buffers were prepared to the desired pH by mixing 0.1 M citric acid with 0.2 M Na_2HPO_4 in varied ratios as shown in Table S1. The pH 8.1 buffer was prepared by dissolving 1.628 g of K_2HPO_4 and 0.089 g of KH_2PO_4 in type 1 water and then diluting to a final volume of 100 mL in a volumetric flask.

2.2. PURIFICATION AND SURFACE MODIFICATION OF ND

To remove non-diamond carbon, 2.0 g of as-received ND were placed into a 50-mL porcelain crucible and heated in air at 425°C for 2 hours in a Thermolyne 2L D1 Benchtop Muffle Furnace (Thermo Scientific).¹⁵ Then, the NDs were refluxed overnight in 50 mL (1:1) volume of 35 wt. % aqueous HCl : 70 wt. % aqueous HNO_3 to remove traces of metals and metal oxides and to hydrolyze surface anhydrides. The mixture was then allowed to cool to ambient temperature. Excess acids were removed by decanting

followed by several cycles of rinsing and centrifuging with deionized water until the pH was neutral. Then, the mixture was dried in a desiccator with drierite under vacuum at ambient temperature for about two days, yielding a purified carboxylated ND (ND-COOH). This ND-COOH was used as a starting material for the synthesis of all other functionalized NDs in this work.

Aminated ND (ND-NH₂) was produced in two stages: 1) conversion of ND-COOH to acyl chloride ND (ND-COCl), 2) reaction of ND-COCl with ethylenediamine (EDA).¹⁶ In the first stage, a mixture of 1.0 g of ND-COOH in a 100 mL round-bottom flask with a Teflon-coated magnetic stirrer bar, 50 mL thionyl chloride (SOCl₂), and 0.5 mL of anhydrous dimethylformamide (DMF) as a catalyst was sonicated in an ultrasonic bath to break all visible ND agglomerates. The flask was then connected to a condenser closed with a drierite-filled drying tube and heated overnight under reflux at ~70 °C to yield ND-COCl. The flask was then cooled to ambient temperature, and excess SOCl₂ was removed by vacuum distillation at ≤ 50 °C to suppress thermal decomposition of SOCl₂. The residual solid was rinsed six times with 50 mL anhydrous THF, and excess THF was decanted. The solid was then dried overnight in a desiccator containing drierite under vacuum at ambient temperature. In the second stage, 1.0 g of dry ND-COCl was mixed with 50 mL anhydrous ethylenediamine in a 100 mL round-bottom flask containing a Teflon coated magnetic stirrer bar. The mixture was sonicated in an ultrasonic bath until all visible agglomerates of nanodiamond disappeared. The flask was then connected to a condenser closed with a drierite drying tube and heated overnight at ~60 °C under reflux. After cooling to ambient temperature, ND-NH₂ powder was precipitated, and excess EDA was gently removed using a pipette. The resulting ND-NH₂

powder was rinsed six times with 50 mL fresh anhydrous THF to remove any traces of adsorbed EDA. A few drops of THF from the last wash were mixed with ~10 mL of deionized water, and the pH of the solution was measured to test for complete removal of EDA, as indicated by neutral pH. The resulting ND-NH₂ was dried on a watch glass at room temperature in ambient air. Aminated ND was characterized as reported before.¹⁶

Hydroxylated ND (ND-OH) was synthesized as described previously.¹⁷ 1.0 g ND-COOH was purged several times with argon gas in a 250-mL Schlenk flask containing a Teflon-coated magnetic stirrer bar. Anhydrous tetrahydrofuran (THF) was degassed by purging with argon gas for one hour. 5 mL of degassed THF was added to the Schlenk flask containing ND-COOH, and the mixture was sonicated to break all visible agglomerates. Then, 10 mL of a 2.0 M solution of lithium aluminum hydride (LiAlH₄) in THF was added. The mixture was stirred overnight at ambient temperature under argon. The excess of (LiAlH₄) was quenched by dropwise addition of 1 M HCl. Then, 1 M KOH was added until neutral pH. The product was rinsed and centrifuged several times with water and finally with acetone. The resulting ND-OH was dried overnight at 90 °C.

2.3. CHARACTERIZATION OF FUNCTIONALIZED ND

Transmission Electron Microscopy (TEM) was carried out using an FEI Tecnai G2 F20 S-TWIN transmission electron microscope equipped with field-emission gun, operated at 200 kV. TEM samples were prepared by drop-casting aqueous ND suspensions onto carbon-coated copper grids followed by drying in the ambient atmosphere. Additional structural information was obtained by small-area electron diffraction (SAED), performed using the same instrument. X-ray diffraction (XRD)

analysis of as-received ND was conducted using a PANalytical X'Pert multipurpose diffractometer (Malvern Instruments, Ltd., Malvern, UK), powered by a Philips PW3064/60 X-ray generator with a Cu K α ($\lambda = 1.540598 \text{ \AA}$) radiation source. Fourier Transform Infrared (FTIR) spectra were recorded using a Thermo Nicolet NEXUS 470 FT-IR Spectrometer, in a range 400-4000 cm^{-1} with 1 cm^{-1} resolution. Pellets were prepared by pressing a mixture of 2 mg ND and 200 mg KBr under a load of 10-15 tons. A Zetasizer Nano ZSP and an MPT-2 multi-purpose titrator (Malvern Instruments, Ltd.) were used to determine ζ -potential and size of the ND agglomerates as a function of pH (ζ -potential titration) at 23 °C. For all NDs, 10 mL of 0.01 wt. % ND colloidal solution was used to measure ζ -potential and average particle size with 0.5 pH steps over a pH range 2.0 – 9.0 with three measurements at each pH. To minimize initial aggregation, for negatively charged ND-COOH the starting pH was 9.0, and for positively charged ND-NH₂ and ND-OH the starting pH was 2.0. The titrator was thoroughly cleaned and primed after every sample measurement to avoid contamination and remove air bubbles, and the pH probe was properly calibrated to ensure accurate results.

2.4. ADSORPTION STUDY

ND stock suspensions were prepared in pre-weighed, reinforced RINO microcentrifuge tubes (Next Advance, NY, USA) by dispersing functionalized NDs in type 1 water at a nominal concentration of 1.4 wt. %. The actual concentration of each stock solution was determined by weighing the NDs and the ND-water suspension. The NDs were dispersed by bombarding the outsides of the RINO tubes in a Bullet Blender Storm (Next Advance) at max speed for 10 min. The tubes were then sonicated in an

ultrasonic bath for 20 min. The tubes containing ND stocks left to equilibrate to room temperature on a rotator. The contents of the tubes were vigorously vortexed immediately before any liquid transfer procedures. The density of each stock ND suspension was determined by weighing aliquots measured out with a volumetric pipette. The density was used to convert the concentration from mg ND/g solution to units of mg/mL. Appropriate dilutions were made to aliquots of ND stocks with type 1 water to yield a working concentration of 2.00 mg/mL. An 804 ppm stock solution of tiopronin was prepared by dissolving 80.4 mg of tiopronin in type 1 water in a 100-mL volumetric flask. All working solutions were prepared by dilutions of this stock solution. In 2-mL microcentrifuge tubes, 500 μ L of 2.00 mg/mL ND working solutions were mixed with 500 μ L of the appropriate working tiopronin solution to produce samples containing 1 mg/mL functionalized ND and 0-200 ppm tiopronin. The samples were thoroughly mixed by vortexing and placed on a rotator for 24 hours. After this time, the samples were placed in a centrifuge and subjected to $12,000 \times g$ for 12 min. The supernatants were collected and centrifuged again at $12,000 \times g$ for 12 min to remove any remaining NDs. Free tiopronin was determined in the supernatant using a sensitive HPLC technique described previously.¹⁸ Briefly, the supernatant was diluted as necessary, and 25 μ L of supernatant was added to 100 μ L of reducing buffer (75 μ M TCEP and 2.5 μ M NAC in pH 7.0 citrate-phosphate buffer). The sample was then derivatized by the addition of 375 μ L of 33 μ M ThioGlo-3. The derivatized sample was acidified by the addition of 5 μ L of 2 M HCl and diluted with 250 μ L of 15 mM H₃PO₄. Finally, the sample was filtered and subjected to HPLC analysis. The calibration standards were processed in parallel with the unknown samples.

2.5. RELEASE STUDY

The release study methodology was adopted from a previous investigation.¹³ NDs were loaded with tiopronin by mixing 6.1 mL of 2.00 mg/mL ND in 15-mL centrifuge tubes with 6.1 mL of 80, 200, or 400 ppm tiopronin for ND-COOH, ND-OH, and ND-NH₂, respectively. These concentrations were selected based on the maximum monolayer adsorption capacity of each ND type, as determined in the adsorption study. The tubes were placed on a rotator for 24 hours to equilibrate. After this time, 12 mL of each loaded ND sample was divided into 12 pre-weighed 2-mL microcentrifuge tubes. The loaded NDs were centrifuged as described previously, and the supernatants were carefully removed with a pipette. The supernatants were analyzed in the same manner as the adsorption samples to determine the amount of tiopronin adsorbed in each sample. To wash away unbound tiopronin, the loaded NDs were rinsed with 1000 μ L of type 1 water. The samples were centrifuged to precipitate the NDs, and the water was carefully removed with a pipette. This step was repeated once more. After washing, the loaded ND precipitates were dried under vacuum in a Vacufuge Concentrator 5301 (Eppendorf, Hauppauge, NY, USA) heated to 60°C. The NDs were left to dry for at least 3 hours, until they had a dry, cracked appearance. The mass of ND remaining in each tube was determined by subtracting the weight of the empty tube from that of the tube with dried NDs. The weight of adsorbed tiopronin molecules was negligible. To investigate the relationship between pH and tiopronin release, the loaded NDs were divided into four groups per ND type (pH 4.0, 5.8, 7.3, and 8.1) with 3 replicates per group. The loaded NDs were resuspended by vortexing in a buffer solution with a pH corresponding to the group. The volume of buffer added was based on the mass of ND remaining in each tube

after rinsing and drying such that the ND concentration would be 1 mg/mL. The tubes were placed on a rotator during the desorption study. Every 24 hours, the tubes were centrifuged to precipitate the NDs as described previously. Sample volumes equal to 15% of the total buffer volume were collected from the supernatant solution for tiopronin analysis. This volume was replaced with an equal volume of fresh buffer, and the NDs were resuspended by vortexing. The tubes were then returned to the rotator. The samples were analyzed for tiopronin in the manner described in previous sections, however, separate calibration standards were prepared for each of the pH 4.0, 5.8, 7.3, and 8.1 buffers to account for matrix effects during analysis (Figures S1-4). Determinations of statistical significance were made using two-way ANOVA followed by a Bonferroni post hoc test using GraphPad Prism 5.

3. RESULTS AND DISCUSSION

3.1. CHARACTERIZATION OF FUNCTIONALIZED ND

Representative TEM micrographs of ND-COOH are shown in Figure 2. Figure 2A shows a low-resolution image of an ND-COOH sample, which reveals typical morphology of detonation nanodiamonds dried on TEM grid. The sample appears uniform, and although separate single nanodiamond particles were found in the sample, larger clusters were primarily observed. The high resolution TEM image of ND-COOH in Figure 2B shows 0.206 nm (111) d-spacing of crystalline diamond. The selected-area electron diffraction (SAED), shown in Figure 2C, confirms the diamond crystalline structure of the ND-COOH particles, with strong SAED rings corresponding to (111),

(220), and (311) planes of ND with d-spacing of 0.206 nm, 0.127 nm, and 0.109 nm, respectively. The measured d-spacing values match well with the structure of cubic diamond. ¹⁹⁻²⁰ XRD of the as-received ND (Figure 3A) shows three prominent peaks consistent with diffraction of diamond at $2\theta = 43.9^\circ$, 75.2° and 91.3° indexed as (111), (220) and (311) planes in cubic diamond.

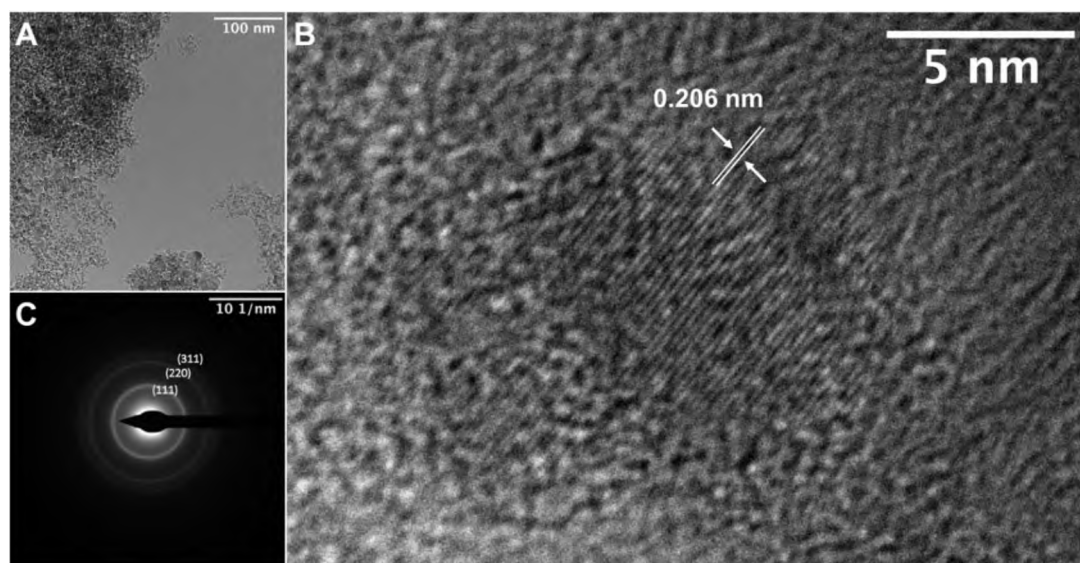


Figure 2. A. Low resolution and B. High resolution TEM micrographs of ND-COOH showing 0.206 nm d-spacing. C. Selected area electron diffraction pattern of ND-COOH sample consistent with small ND primary particle size and diffraction rings corresponding to the (111), (220), and (311) planes of diamond.

Surface chemistry of ND, ND-COOH, ND-OH and ND-NH₂ was characterized by FTIR spectroscopy (Figure 3B-C). Figure 3C confirms covalent bonding of amino groups to ND surface in ND-NH₂. The peaks at 3418 cm^{-1} present in all ND spectra correspond to O-H stretching vibrations and could be assigned to O-H or adsorbed water.²¹ The C-H stretch bands at ~ 2870 and $\sim 2923\text{ cm}^{-1}$ originate from hydrogen atoms attached to ND surface, as well as from CH₂ groups of EDA in ND-NH₂. The bands at

1637 cm^{-1} and $\sim 3418 \text{ cm}^{-1}$ in ND-NH₂ arise from the bending and stretching modes of N-H as well as remaining O-H bonds.²¹⁻²² ND-NH₂ amide peaks correspond to blue-shifted Amide I (1667 cm^{-1}) and Amide II (1520 cm^{-1}), as well as Amide III ($\sim 1320 \text{ cm}^{-1}$) (Figure 3C).²² A small C=O band at 1776 cm^{-1} in ND-NH₂, suggests the presence of carbonyl species (carboxylic acids, ketones, esters, etc.) in the ND-NH₂.¹⁶

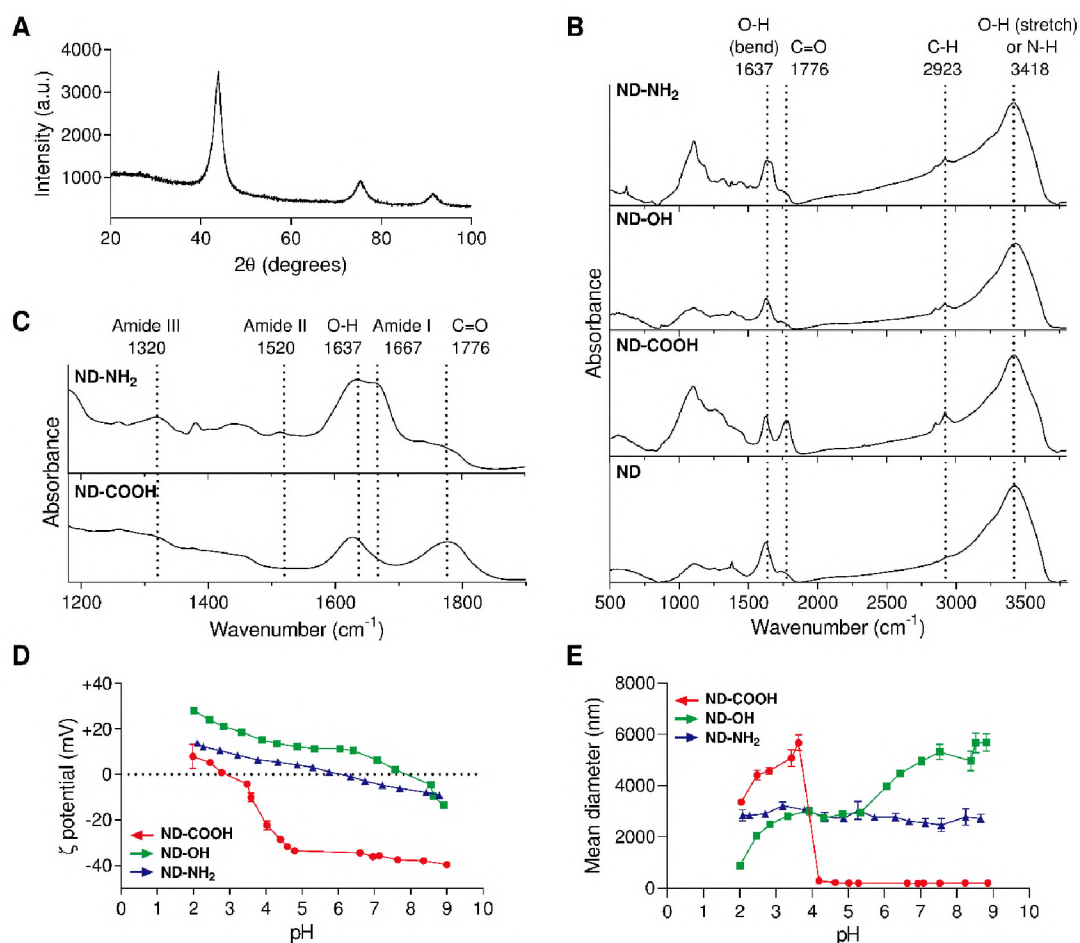


Figure 3. A. XRD pattern of as-received ND. B. FTIR spectra of as-received ND, ND-COOH, ND-OH, and ND-NH₂. C. FTIR spectra of ND-COOH and ND-NH₂ in the range of wavelength corresponding to Amide bands. Dashed lines indicate absorbance corresponding to major functional groups D. ζ -potential vs. pH and E. Mean diameter of ND agglomerates vs. pH for ND-COOH (●), ND-OH (■), and ND-NH₂ (▲). Reported as mean \pm standard deviation. Arrows indicate direction of titration for each type of ND.

The effect of pH on ζ -potential was investigated for ND-COOH, ND-OH, and ND-NH₂ (Figure 3D) to make predictions about electrostatic interactions between tiopronin and NDs. ND-COOH has a strongly negative ζ -potential above pH 3.8 due to deprotonation of ND-COOH to ND-COO⁻. ND-OH has a moderately positive ζ -potential in acidic and neutral pH with an isoelectric pH 7.9, above which a negative ζ -potential was observed. The positive ζ -potential in acidic pH may result from ND-OH protonation or the presence of hydrogen terminations (ND-H) formed during the preparation of ND-OH. ND-H has been previously reported to exhibit a highly positive ζ -potential for reasons that are not entirely clear.²²⁻²³ ND-NH₂ has a weakly positive ζ -potential in acidic pH with an isoelectric pH 6.1, above which it has a weakly negative ζ -potential. Although ND-NH₂ is expected to have a more strongly positive ζ -potential in acidic pH compared to ND-OH, contribution from remaining COOH groups in ND-NH₂ (also seen in FTIR) results in a surface with mixed electrostatic affinity and a lower net ζ -potential. The effect of pH on the size of ND agglomerates was also investigated. The results are shown in Figure 3E. For ND-COOH, pH had a significant impact on the extent of agglomeration. The nominal size of ND-COOH clusters was 200 nm for pH > 4. Below pH 4, significant aggregation of ND-COOH was observed, with particle sizes ranging from 3.4 to 5.7 μ m. This observation can be attributed to protonation of the carboxylate group, resulting in reduction of the magnitude of ζ -potential as indicated in Figure 3D and, consequently, a significant decrease in colloidal stability. For ND-OH, average size increased with increasing pH, with sizes ranging from 0.8 to 5.7 μ m. This is also in agreement with the ζ -potential titration data, which shows that the magnitude of ND-OH ζ -potential drops with increasing pH, leading to weaker electrostatic repulsion between individual particles

which confers colloidal stability. For ND-NH₂, the effect of pH on size was much less pronounced. The average diameter of ND-NH₂ agglomerates ranged from 2.5 to 3.2 μm. This result is reasonable considering ND-NH₂ has a mix of carboxylate and amine surface moieties and exhibited only small changes in net ζ-potential over the tested pH range.

3.2. ADSORPTION OF TIOPRONIN

Adsorption isotherms were constructed by plotting the equilibrium tiopronin concentration (C_{eq}) following adsorption vs. A , the amount of adsorbed drug per gram of ND, calculated by taking the difference of the tiopronin initial solution concentration (C_0) and the equilibrium concentration after 24 hours. The experimental adsorption isotherms (Figure 4) were fit by nonlinear least-squares regression to Langmuir and Freundlich models. The Langmuir model (Equation 1) assumes that all adsorption sites are identical with respect to affinity for adsorbate and energy of adsorption.

$$A = A_{max} \frac{K_L C_{eq}}{1 + K_L C_{eq}} \quad (1)$$

This model also assumes that all adsorbed molecules are in contact with the adsorbent (i.e., monolayer adsorption).²⁵ In Equation 1, A_{max} represents the maximum monolayer adsorption capacity of the adsorbent, and K_L represents the strength of binding. The Freundlich model (Equation 2), in contrast, accommodates multilayer adsorption and adsorbent surface heterogeneity.²⁶ In this empirical model, K_F and n are relative indicators of adsorption capacity and favorability, respectively.

$$A = K_F C_{eq}^{1/n} \quad (2)$$

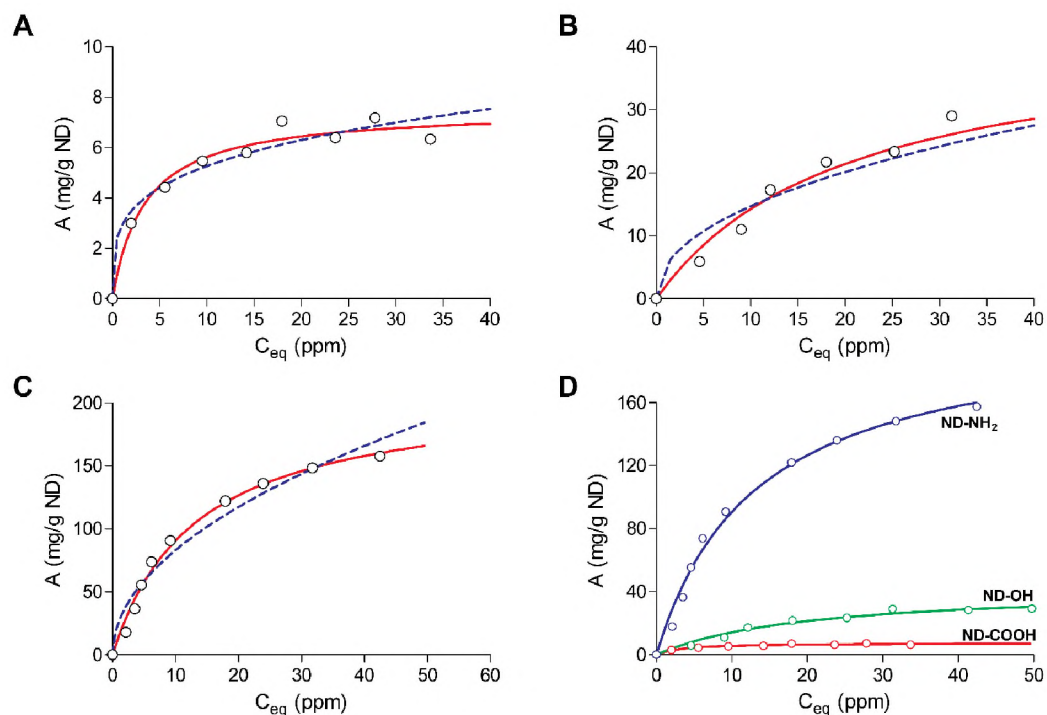


Figure 4. A-C. Langmuir (solid red line) and Freundlich (blue dashed line) fits to experimental adsorption isotherms of A. ND-COOH, B. ND-OH, and C. ND-NH₂. D. Overlay of Langmuir fits from A-C.

For all three NDs, R values for adsorption data fits to either model are all greater than 0.97. A_{max} values for NDs change in the following order: ND-COOH < ND-OH < ND-NH₂ (Table 1). The same trend is observed for K_F values. Neither the Langmuir binding strength K_L nor the Freundlich adsorption favorability parameter n follows this trend: both are highest for ND-COOH, but ND-OH has the lowest K_L , while ND-NH₂ has the lowest n . Overall, the Langmuir model fits the experimental data more closely than the Freundlich model for all three NDs investigated here. This indicates that the interaction of tiopronin with the ND surface may be understood largely in terms of the Langmuir model and monolayer adsorption. Specifically, the parameters A_{max} and K_L derived from this model can be used to compare the properties of functionalized NDs as

adsorbents for tiopronin and to predict their relative effectiveness for different applications. Parameters for each of the fits, as well as the resulting Pearson's correlation coefficients (R) are shown in Table 1.

Table 1. Parameters and Pearson's correlation coefficient for Langmuir and Freundlich curve fits to adsorption data

ND	Langmuir			Freundlich		
	A_{max} (mg/g)	K_L (mL/mg)	R	n	K_F	R
COOH	7.54	295	0.986	3.87	17.3	0.976
OH	42.9	49.8	0.989	2.21	118	0.971
NH ₂	210	76.2	0.996	2.01	824	0.980

Tiopronin is a weak acid, with a -COOH pK_a of 3.9. Therefore, a significant proportion of the dissolved tiopronin will become negatively charged in water. ND-COOH exhibits negative ζ -potential. Thus, the low monolayer adsorption capacity of the ND-COOH may be explained by electrostatic repulsion between the deprotonated ND-COO⁻ and the deprotonated tiopronin. The high adsorption capacity of the ND-NH₂ may be the result of other factors. Under the mildly acidic conditions of the adsorption studies, ND-OH possesses a more strongly positive ζ -potential than ND-NH₂ (Figure 3D), yet it has a lower A_{max} . This suggests that the higher adsorption capacity of ND-NH₂ cannot be explained solely in terms of electrostatic attraction between positively charged surface functional groups and tiopronin. It therefore becomes necessary to consider the effects of colloidal stability on available adsorption sites. Agglomerates formed more readily by less positively charged ND-NH₂ exhibit greater variation in available adsorption sites, including areas where tiopronin may accumulate and be trapped, leading to greater apparent A_{max} and binding strength of ND-NH₂.²⁷ While exhibiting a stronger electrostatic

attraction to the anionic tiopronin, the greater net positive charge, in addition to the capacity for extensive hydrogen bonding with water, is thought to stabilize the ND-OH particles in the suspension, resulting in less agglomeration and fewer such sites of hindered desorption.

Figure 5 shows a plot of A_{max} vs. K_L for NDs with different surface chemistries studied here. Although the underlying mechanisms have not been well-established for the vast majority of drug-ND systems, the apparent discrepancy between drug binding strength and adsorption capacity has been reported before^{13-14, 26} and indicates that these characteristics may be independently tailored to meet the needs of different applications. The ability to design ND drug delivery systems wherein both loading capacity and binding strength can be modified to suit the application is extremely attractive, as safe and effective delivery of drugs with different potencies and toxicities warrant highly tailorable vehicles that can carry and release the drug as required. Furthermore, the gap between acknowledgment of their evident utility and command of the mechanisms responsible, may provide greater impetus for further investigations of ND theranostic platforms.

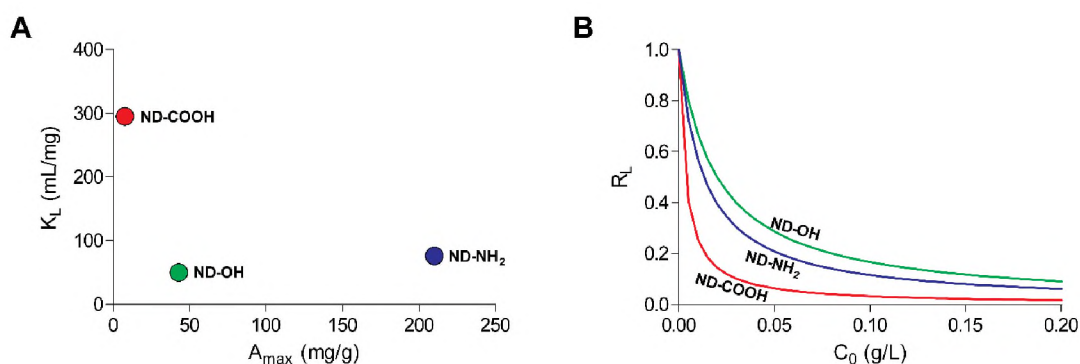


Figure 5. A. K_L vs. A_{max} B. Separation factor R_L vs. C_0

Separation factor R_L is related to K_L by equation 3, where C_0 is the initial concentration of adsorbate. The value of R_L indicates whether adsorption is irreversible ($R_L = 0$), favorable ($0 < R_L < 1$), or unfavorable ($R_L > 1$) at the initial concentration of adsorbate.²⁸

$$R_L = \frac{1}{1+K_L C_0} \quad (3)$$

Given that K_L values ranged from 76.2 and 295 mL/mg, R_L values approach 1 as C_0 approaches 0 mg/mL and 0 as C_0 approaches infinity. Therefore, adsorption of tiopronin onto functionalized ND is favorable at any concentration and becomes more favorable as concentration increases.²⁹

3.3. RELEASE STUDY

Tiopronin is negatively charged at physiological pH (7.4), and therefore cannot readily cross the phospholipid bilayer of most cell membranes by passive diffusion. ND-mediated delivery of tiopronin across the membranes in a form of a thin (monomolecular) adsorbed layer may circumvent this problem, while potentially improving bioavailability of the drug. In addition, since both tiopronin and functionalized NDs have pH-labile protons, we examined the potential for pH-triggered release of tiopronin from NDs. Tiopronin-loaded ND-COOH, ND-OH, and ND-NH₂ were dispersed at 1 mg/mL in buffers ranging from pH 4.0 to 8.1. The amount of tiopronin released was measured daily for the first ten days after which measurements were taken every 2-3 days. No significant release was observed beyond 12 days. To understand the effect of pH on tiopronin release for each functionalized ND, the cumulative release as a percentage of adsorbed tiopronin

was plotted vs. time (Figure 6A-C). Additionally, cumulative release after 1 day and 12 days was compared across the different ND surface chemistries (Figure 6D-E).

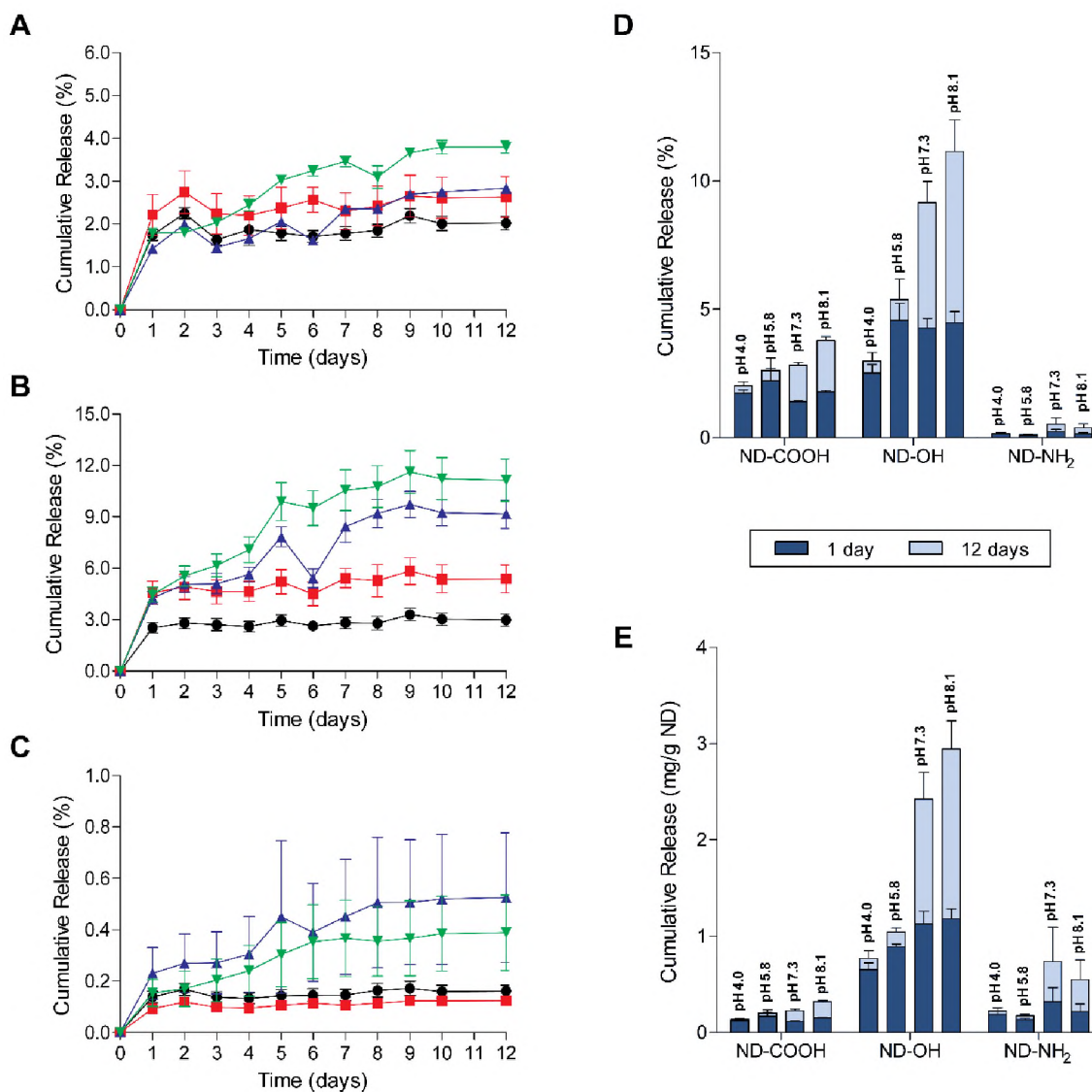
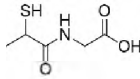
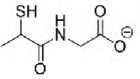
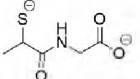


Figure 6. A-C. Plots of cumulative tiopronin release as a percentage of the initial amount of adsorbed tiopronin vs. time for A. ND-COOH, B. ND-OH, and C. ND-NH₂ in pH 4.0 (●), 5.8 (■), 7.3 (▲), and 8.1 (▼) buffer. Error bars are standard error of the mean (σ/\sqrt{n}). D-E. Cumulative tiopronin release after 1 day and 12 days, expressed as D. percentage of the initial amount of adsorbed tiopronin and E. mass of tiopronin released per gram of ND. The error bars are standard error of the mean. The pH of the desorption buffer is indicated above each corresponding bar.

Table 2. Calculated distribution of tiopronin microspecies and ζ -potential of ND suspensions

pH	Estimated Microspecies Distribution (%)*			ζ -potential (mV)		
				ND-COOH	ND-OH	ND-NH ₂
4.0	42.27%	57.73%	0.00%	-22.6	+14.5	+5.95
5.8	1.15%	98.82%	0.03%	-34.1	+11.3	+0.86
7.3	0.04%	99.08%	0.88%	-36.2	+4.46	-4.99
8.1	0.01%	94.64%	5.35%	-37.8	-1.57	-7.23

*Chemicalize from ChemAxon was used for calculation of estimated microspecies distribution, Feb, 2019, <https://chemicalize.com>

Table 2 shows calculated microspecies distribution of tiopronin and ζ -potentials determined for each functionalized ND at relevant pH levels. The majority of tiopronin is negatively charged over the tested pH range, with > 57% deprotonated at pH 4.0 and > 99% deprotonated at pH 5.8 – 8.1. Thus, it was expected that release will generally increase under higher pH conditions which reduce the number of positive charges on the ND surface.

Figure 6A shows that pH had a minimal effect on the total amount of tiopronin released from ND-COOH. The difference in means with respect to release was statistically significant only between pH 4.0 and 8.1, but only after 5 days. This result is unsurprising since ND-COOH retains a highly negative ζ -potential, even at pH 4.0. For this reason, ND-COOH may be useful for applications which require pH-independent release of tiopronin. It is also worth mentioning that because of the large number of negative surface charges on ND-COOH, it is much easier to maintain a small particle size distribution; even single-digit NDs can be prepared from ND-COOH without milling using salt-assisted ultrasonic deaggregation (SAUD).³⁰ The pH also had a minimal effect

on the release of the tiopronin from ND-NH₂ (Figure 6C). The difference in means can only be considered statistically significant between pH 6 and 7, and only after 8 days. The ζ -potential plot in Figure 3D suggests that a number of COOH moieties remain on the surface of ND-NH₂. These groups are negatively charged within the pH range used in this study, contributing to the net surface charge and resulting in a low magnitude ζ -potential. Although the means suggest that more release occurs at pH 4.0 than at pH 5.8, the difference between the means is statistically insignificant. The same is true for the means of pH 7.3 and 8.1. From a practical standpoint, no appreciable difference in release will be achieved by varying pH in the range of 4-8 for ND-NH₂ or ND-COOH. The pH had the greatest effect on tiopronin release from ND-OH. The effect of pH on release follows a predictable trend with lower pH resulting in slower release. This effect starts to become significant after 3-4 days.

Figure 6D shows that ND-OH released the greatest amount of tiopronin in terms of percent relative to the amount adsorbed (2.6 – 13.1%) while ND-COOH released 1.8 – 4.0%, and ND-NH₂ released only 0.1 – 1.0%. However, due to the large differences in adsorption capacity, it is also worth comparing the mass of tiopronin that can be released per gram of loaded ND. Figure 6E shows that ND-OH also released the greatest amount of drug per gram of loaded ND (0.68 – 3.3 mg/g) while ND-NH₂ released more drug than an equal weight of ND-COOH (0.14 – 1.4 mg/g from ND-NH₂ vs. 0.12 – 0.34 mg/g from ND-COOH), owing to the large difference in adsorption capacity. Finally, it appears that prolonged release of tiopronin from ND-OH is possible under neutral or alkaline pH conditions since the concentration of free tiopronin continues to increase substantially several days after the start of the desorption experiments. In contrast, acidic conditions

retard continued release of tiopronin beyond that which is released initially. This trend is present in each of the functionalized NDs, and the effect can be considered statistically significant in ND-OH as determined by a Bonferroni *post hoc* test. This may be beneficial for delivery of tiopronin and other thiol antioxidants since their premature oxidation is a concern. ND-OH may slowly release tiopronin in the acidic environment of the stomach. Blood plasma is buffered at pH 7.4, allowing for increased drug release after entering the bloodstream. Additionally, weakly acidic formulations may be prepared which can prevent premature release and oxidation of the drug in topical formulations.

4. CONCLUSION

Adsorption and release of tiopronin is sensitive to the changes of ND surface chemistry. However, due to the complexity of interactions between surface functional groups, drug molecules, and the environment, this effect cannot be explained by simply examining net surface charges. Our results show that ND-OH provides the best balance between drug capacity and release, making it the best candidate for applications which benefit from prolonged release of large amounts of tiopronin. Furthermore, formulations of loaded ND-OH can be prepared at an acidic pH which may be able to prevent premature release and degradation of tiopronin. ND-COOH has a lower adsorption capacity but can provide moderate release independent of pH. Additionally, ND-COOH is easily dispersed due to electrostatic repulsion and high magnitude of ζ -potential, so it may be best suited for applications that require low agglomeration and can benefit from high surface area of ND. Finally, desorption of tiopronin may not be necessary for all

applications, so although ND-NH₂ only releases a small portion of its payload, it has a very high capacity and may be useful in applications in which it is desirable to have tiopronin attached on the surface of dispersed ND for prolonged release or storage in the body with subsequent local release triggered by topical application of ultrasound, light, heat, and other stimuli.

FUNDING

This work was supported by the NEI of the National Institutes of Health under award number R15EY029813 and the Richard K. Vitek/FCR Endowment Missouri University of Science and Technology. The content is solely the responsibility of the authors and does not necessarily represent the official views of the National Institutes of Health.

AUTHOR CONTRIBUTIONS

VM and NE conceived and supervised the project. JB and AP designed and executed adsorption and release experiments and performed data analysis. IA functionalized ND surfaces and performed all ND characterization experiments. AC assisted with adsorption and release experiments. VM provided guidance and supervision during all stages of ND synthesis, characterization, adsorption and release. NE was instrumental in selection of antioxidant drug and oversaw analysis of adsorption and release. All authors have approved the final article.

DECLARATIONS OF INTEREST

None

SUPPORTING INFORMATION

Methodology for the preparation of citrate-phosphate desorption buffers is provided in Table S1. The pH 8.1 buffer used for desorption experiments was prepared by dissolving 1.628 g of K_2HPO_4 and 0.089 g of KH_2PO_4 in type 1 water and then diluting to a final volume of 100 mL in a volumetric flask as mentioned in Section 2.1.

Sample calibration curves used for the determination of MPG in desorption buffers, as described in Section 2.5, are shown in Figures S2-S5. Matrix effects were significant among the different buffers, but peak areas were strongly correlated to [MPG] in each buffer.

Table S1. Preparation of citrate-phosphate buffers

pH	0.1 M Citric acid (mL)	0.2 M Na_2HPO_4 (mL)
4.0	61.45	38.55
5.8	39.55	60.45
7.0	17.65	82.35
7.3	13.05	86.95

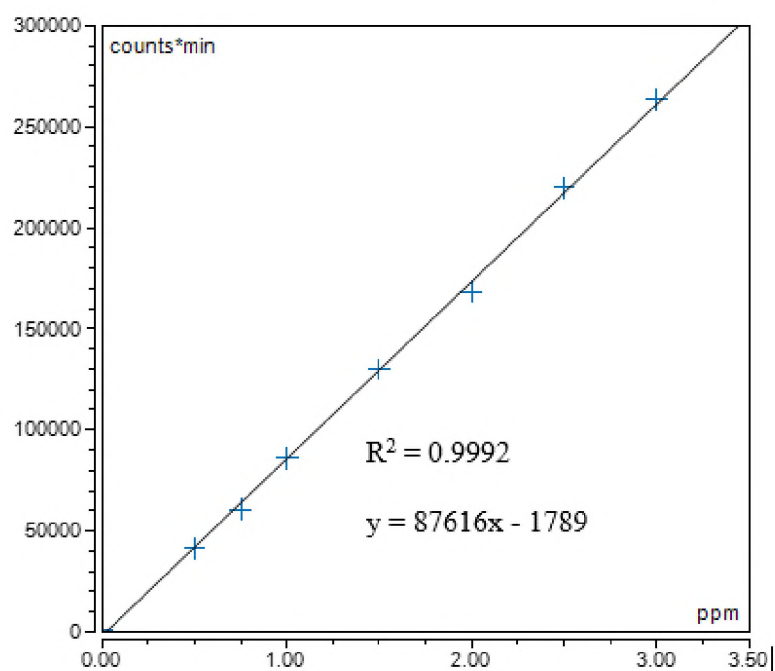


Figure S1. Calibration curve for tiopronin in pH 4.0 desorption buffer

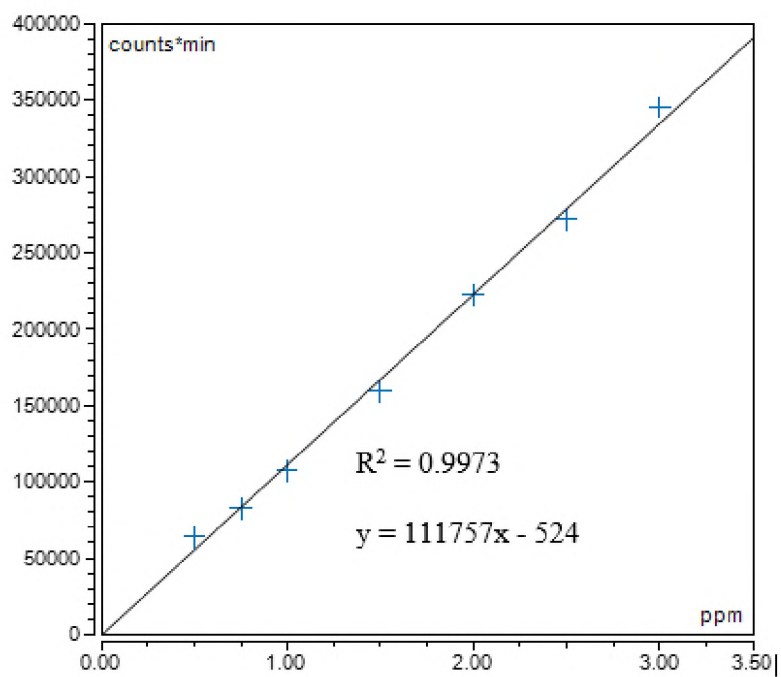


Figure S2. Calibration curve for tiopronin in pH 5.8 desorption buffer

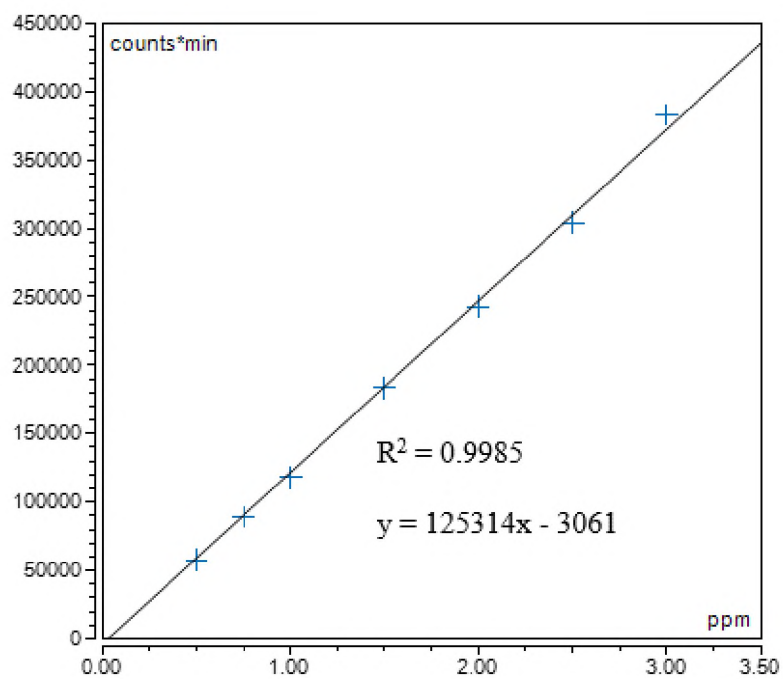


Figure S3. Calibration curve for tiopronin in pH 7.3 desorption buffer

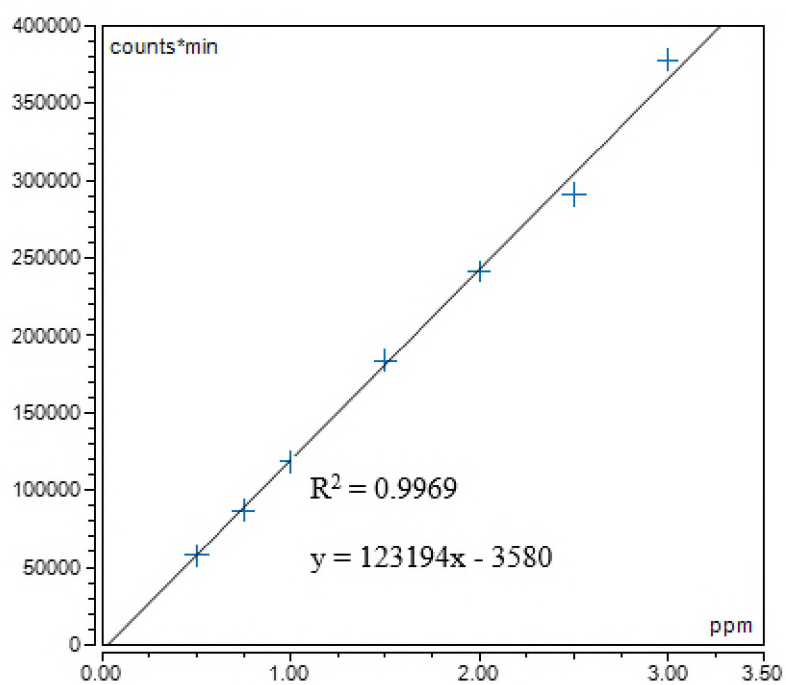


Figure S4. Calibration curve for tiopronin in pH 8.1

REFERENCES

1. Castañeda-Arriaga, R.; Vivier-Bunge, A.; Raul Alvarez-Idaboy, J. Primary antioxidant and metal-binding effects of tiopronin: A theoretical investigation of its action mechanism. *Comput. Theor. Chem.* **2016**, *1077*, 48-57.
2. Kobayashi, S.; Kasuya, M.; Ishii, Y.; Takehana, M.; Sakai, K.; Suzuki, N.; Itoi, M. Effects of 2-mercaptopropionylglycine on the development of X-ray-induced cataract in rats. *Curr. Eye Res.* **1992**, *11* (11), 1099-103.
3. Ichikawa, H.; Imaizumi, K.; Tazawa, Y.; Obara, Y.; Ishikawa, Y.; Tobar, I.; Tanabe, Y. Effect of tiopronin on senile cataracts. A double-blind clinical study. *Ophthalmologica* **1980**, *180* (5), 293-8.
4. Kuck, J. F., Jr.; Kuck, K. D. The Emory mouse cataract: the effects on cataractogenesis of alpha-tocopherol, penicillamine, triethylenetetramine, and mercaptopropionylglycine. *J. Ocul. Pharmacol.* **1988**, *4* (3), 243-51.
5. Zhang, J. G.; Lindup, W. E. Tiopronin protects against the nephrotoxicity of cisplatin in rat renal cortical slices in vitro. *Toxicol. Appl. Pharmacol.* **1996**, *141* (2), 425-33.
6. Järvinen, K.; Järvinen, T.; Urtili, A. Ocular absorption following topical delivery. *Adv. Drug Del. Rev.* **1995**, *16* (1), 3-19.
7. Abdelkader, H.; Alany, R. G.; Pierscionek, B. Age-related cataract and drug therapy: opportunities and challenges for topical antioxidant delivery to the lens. *J. Pharm. Pharmacol.* **2015**, *67* (4), 537-50.
8. Jiang, T.-Y.; Sun, C.-S.; Shen, X.; Wang, T.-Y.; Wang, S.-L. Development of a poloxamer analogs/bioadhesive polymers-based in situ gelling ophthalmic delivery system for tiopronin. *J. Appl. Polym. Sci.* **2009**, *114* (2), 775-783.
9. Hoare, T. R.; Kohane, D. S. Hydrogels in drug delivery: Progress and challenges. *Polymer* **2008**, *49* (8), 1993-2007.
10. Mochalin, V. N.; Shenderova, O.; Ho, D.; Gogotsi, Y. The properties and applications of nanodiamonds. *Nat. Nanotechnol.* **2011**, *7* (11), 11-23.
11. Turcheniuk, K.; Mochalin, V. N. Biomedical applications of nanodiamond (Review). *Nanotechnology* **2017**, *28* (25), 252001.
12. Setyawati, M. I.; Mochalin, V. N.; Leong, D. T. Tuning endothelial permeability with functionalized nanodiamonds. *ACS Nano* **2016**, *10* (1), 1170-81.

13. Giammarco, J.; Mochalin, V. N.; Haeckel, J.; Gogotsi, Y. The adsorption of tetracycline and vancomycin onto nanodiamond with controlled release. *J. Colloid Interface Sci.* **2016**, *468*, 253-261.
14. Mochalin, V. N.; Pentecost, A.; Li, X. M.; Neitzel, I.; Nelson, M.; Wei, C.; He, T.; Guo, F.; Gogotsi, Y. Adsorption of drugs on nanodiamond: toward development of a drug delivery platform. *Mol. Pharm.* **2013**, *10* (10), 3728-35.
15. Osswald, S.; Yushin, G.; Mochalin, V.; Kucheyev, S. O.; Gogotsi, Y. Control of sp²/sp³ carbon ratio and surface chemistry of nanodiamond powders by selective oxidation in air. *J. Am. Chem. Soc.* **2006**, *128* (35), 11635-42.
16. Mochalin, V. N.; Neitzel, I.; Etzold, B. J. M.; Peterson, A.; Palmese, G.; Gogotsi, Y. Covalent incorporation of aminated nanodiamond into an epoxy polymer network. *ACS Nano* **2011**, *5* (9), 7494-7502.
17. Hens, S. C.; Cunningham, G.; Tyler, T.; Moseenkov, S.; Kuznetsov, V.; Shenderova, O. Nanodiamond bioconjugate probes and their collection by electrophoresis. *Diamond Relat. Mater.* **2008**, *17* (11), 1858-1866.
18. Beltz, J.; Pfaff, A.; Ercal, N. Simultaneous determination of tiopronin and its primary metabolite in plasma and ocular tissues by HPLC. *Biomed. Chromatogr.* **2018**, e4375.
19. Reineck, P.; Lau, D. W. M.; Wilson, E. R.; Fox, K.; Field, M. R.; Deeleepojananan, C.; Mochalin, V. N.; Gibson, B. C. Effect of surface chemistry on the fluorescence of detonation nanodiamonds. *ACS Nano* **2017**, *11* (11), 10924-10934.
20. Petit, T.; Puskar, L. FTIR spectroscopy of nanodiamonds: Methods and interpretation. *Diamond Relat. Mater.* **2018**, *89*, 52-66.
21. Mayo, D. W.; Miller, F. A.; Hannah, R. F. *Course Notes on the Interpretation of Infrared and Raman Spectra*. John Wiley & Sons, Inc.: 2004.
22. Petit, T.; Puskar, L.; Dolenko, T.; Choudhury, S.; Ritter, E.; Burikov, S.; Laptinskiy, K.; Brzustowski, Q.; Schade, U.; Yuzawa, H.; Nagasaka, M.; Kosugi, N.; Kurzyp, M.; Venerosy, A.; Girard, H.; Arnault, J.-C.; Osawa, E.; Nunn, N.; Shenderova, O.; Aziz, E. F. Unusual water hydrogen bond network around hydrogenated nanodiamonds. *J. Phys. Chem. C Nanomater. Interfaces* **2017**, *121* (9), 5185-5194.
23. Williams, O. A.; Hees, J.; Dieker, C.; Jager, W.; Kirste, L.; Nebel, C. E. Size-dependent reactivity of diamond nanoparticles. *ACS Nano* **2010**, *4* (8), 4824-30.
24. Langmuir, I. The constitution and fundamental properties of solids and liquids. Part I. Solids. *JACS* **1916**, *38* (11), 2221-2295.

25. Freundlich, H.; Hatfield, H. *Colloid and Capillary Chemistry*. Methuen: London, 1926.
26. Gibson, N. M.; Luo, T.-J. M.; Shenderova, O.; Koscheev, A. P.; Brenner, D. W. Electrostatically mediated adsorption by nanodiamond and nanocarbon particles. *J. Nanopart. Res.* **2012**, *14* (3).
27. Hall, K. R.; Eagleton, L. C.; Acrivos, A.; Vermeulen, T. Pore- and solid-diffusion kinetics in fixed-bed adsorption under constant-pattern conditions. *Ind. Eng. Chem. Fundam.* **1966**, *5* (2), 212-223.
28. Sun, C.-J.; Sun, L.-Z.; Sun, X.-X. Graphical evaluation of the favorability of adsorption processes by using conditional langmuir constant. *Ind. Eng. Chem. Res.* **2013**, *52* (39), 14251-14260.
29. Turcheniuk, K.; Trecuzzi, C.; Deelepojananan, C.; Mochalin, V. N. Salt-assisted ultrasonic deaggregation of nanodiamond. *ACS Appl. Mater. Interfaces* **2016**, *8* (38), 25461-8.

SECTION

2. CONCLUSIONS

Our long term goal is to develop an eye drop formulation that can delay the onset of cataracts. Antioxidant compounds have the potential to mitigate the oxidative damage associated with cataractogenesis, but achieving sufficient concentrations in the lens has proven difficult. In pursuit of this goal, our group is investigating the potential of ND as a platform for improving MPG residence in the eye and reducing levels of reactive oxygen species and oxidative damage associated with cataract. Each investigation presented in this dissertation aimed to address a specific research question.

2.1. TO WHAT EXTENT DOES MPG PROTECT CELLS AGAINST ACUTE OXIDATIVE INSULT?

Oxidative stress was induced in A549 cells by exposure to 0.6 mM *t*BHP. In untreated cells, 0.6 mM *t*BHP resulted in a significant loss of cell viability due to the increased generation of intracellular ROS and mitochondrial superoxide, resulting in GSH depletion. Cells that were simultaneously treated with 0.6 mM *t*BHP and 5 mM MPG were comparable to healthy cells; however, lower doses of MPG were much less effective at preventing cell death. Preservation of cell viability by MPG is most likely the result of direct ROS scavenging, and it is clear that relatively high doses need to be maintained in order for MPG to be effective in this model. However, when interpreting these results, it is important to consider the limitations of the model used. The cells used in this study were from a human lung carcinoma cell line, which is not intended or

expected to fully recapitulate human lenses. Furthermore, the intense, short-lived oxidative insult resulting from incubating the cells in *t*BHP is not representative of the gradual damage accumulated over a lifetime of exposure to relatively low concentrations of oxidants. More complex models studied over a much longer time would be needed in order to draw any conclusions with respect to anticataract efficacy. These experiments are reserved for later stages of drug development. Instead, the experiments discussed here served as a pilot study for establishing a benchmark for MPG's antioxidant activity in a simplified epithelial cell model. These results can serve as a basis for comparison against formulations composed of MPG adsorbed onto ND, but investigations with more complex models are certainly warranted. Future investigations exploring the antioxidant activity of MPG vs. ND:MPG will utilize human lens epithelial cells, corneal epithelial cells, and animal models.

2.2. HOW WILL MPG BE MEASURED IN CELL AND ANIMAL MODELS?

An HPLC method was developed for the determination of MPG and MPA in ocular tissues and other matrices. Pre-column derivatization and fluorescence detection allowed for high sensitivity, and the use of a 4.6- μ m core-shell stationary phase resulted in rapid separation. Method validation experiments demonstrated that this method would be suitable for monitoring MPG uptake and residence in the lens and cornea. Other methods were available for MPG, but they were not suitable for our application either due to sensitivity limitations or matrix interferences. This method is a necessary tool for determining the efficacy of various drug delivery vehicles, as well as the fate of MPG after administration to the eye. This method offers simultaneous determination of MPA,

the primary metabolite of MPG. One of the primary reasons MPG was selected for investigating ND-mediated delivery is that it is metabolized to MPA, making its fate easy to track. Other thiol drug candidates may be more effective as antioxidants, such as the GSH prodrug N-acetylcysteine amide (NACA) because they can increase the size of the total GSH pool in addition to directly scavenging ROS. However, NACA is de-acetylated *in vivo* to N-acetylcysteine (NAC), which is then further metabolized to cysteine, which is used not only for GSH synthesis but also for a number of other biological reactions. Tracking all of these metabolites without radiolabeling would be very difficult and resource-intensive. In contrast, MPG and MPA are not found in untreated human or animal lenses, making efforts to track MPG far more reliable.

2.3. WHAT IS THE OPTIMAL ND SURFACE CHEMISTRY FOR ADSORPTION AND RELEASE OF MPG?

Nanodiamond powder was functionalized to produce ND-COOH, ND-OH, and ND-NH₂, and the effect of surface chemistry on adsorption and desorption of MPG was determined. It would seem from these experiments that ND-OH is the most promising candidate for ND-mediated delivery of tiopronin. The ND-OH provided the best balance between adsorption capacity and sustained release. Furthermore, its release was shown to be the most strongly influenced by pH. Relatively low amounts of MPG were released from ND-OH in slightly acidic conditions, even after 12 days, but ND-OH released large amounts of MPG at physiological pH (7.4) and under slightly basic conditions. Since the cornea can tolerate eye drop formulations as acidic as pH 4, acidic preparations of ND-OH:MPG can prevent premature release and degradation of MPG. Upon administration to the eye, the pH will equilibrate with that of the ocular surface and tear film, triggering

prolonged release of greater amounts of MPG. Finally, ND-OH exhibits a positive ζ -potential at physiological pH, which may help prolong retention of ND-OH:MPG on the cornea due to electrostatic attraction to the negatively charged corneal surface.

Although ND-OH seems like a clear choice for ND-mediated delivery of MPG, there are other factors to consider when optimizing ND surface chemistry for this application. For example, it is unclear at this time whether or not MPG needs to be desorbed from the ND in order to act as a scavenger of ROS. If adsorption to ND does not impede antioxidant activity, then ND-NH₂ may perform even better than ND-OH since ND-NH₂ can carry significantly greater amounts of MPG.

2.4. FUTURE DIRECTIONS

The contents of this dissertation represent the preliminary work necessary for the development and evaluation of ND for delivery of MPG to the eye. The tools developed here will play an integral role in the assessment of ND efficacy. Moving forward, several factors need to be considered for the successful application of ND:MPG in eye drop formulations aimed at delaying cataract. Firstly, it is important to investigate the effect of ND on the antioxidant activity of MPG to ensure that the ND does not hinder its ability to scavenge ROS and to determine whether ND can preserve or even promote the action of MPG. Another key step forward is to determine the effect of ND on corneal penetration and lenticular uptake of MPG with appropriate cell and animal models.

After optimization of the ND:MPG eye drop formulation, it should be tested in an animal model of age-related nuclear cataract. As of now, there is no animal or cell model that fully recapitulates every relevant feature of human cataractogenesis; however, the

Emory mouse model is recommended. Cataract development in these animals mimics important features of human age-related nuclear cataract. In contrast with models that employ short-lived, high-intensity oxidative insults to induce cataracts, Emory mice develop cataracts spontaneously over the course of 5-6 months. This gradual progression provides a window for monitoring pre-cataractous changes and the effects of preventative treatments.

BIBLIOGRAPHY

1. Pascolini, D.; Mariotti, S. P., Global estimates of visual impairment: 2010. *The British journal of ophthalmology* **2012**, *96* (5), 614-8.
2. Yorston, D., Cataract complications. *Community Eye Health* **2008**, *21* (65), 1-3.
3. Lim, J. C.; Umopathy, A.; Grey, A. C.; Vaghefi, E.; Donaldson, P. J., Novel roles for the lens in preserving overall ocular health. *Exp Eye Res* **2017**, *156*, 117-123.
4. Mahendiran, K.; Elie, C.; Nebel, J. C.; Ryan, A.; Pierscionek, B. K., Primary sequence contribution to the optical function of the eye lens. *Sci Rep* **2014**, *4*, 5195.
5. Hoehenwarter, W.; Klose, J.; Jungblut, P. R., Eye lens proteomics. *Amino Acids* **2006**, *30* (4), 369-389.
6. Bloemendal, H.; de Jong, W.; Jaenicke, R.; Lubsen, N. H.; Slingsby, C.; Tardieu, A., Ageing and vision: structure, stability and function of lens crystallins. *Prog Biophys Mol Biol* **2004**, *86* (3), 407-85.
7. Truscott, R. J., Age-related nuclear cataract-oxidation is the key. *Exp Eye Res* **2005**, *80* (5), 709-25.
8. Lou, M. F., Redox regulation in the lens. *Prog Retin Eye Res* **2003**, *22* (5), 657-682.
9. Reddy, V. N., Glutathione and its function in the lens—An overview. *Exp Eye Res* **1990**, *50* (6), 771-778.
10. Truscott, R. J.; Augusteyn, R. C., Oxidative changes in human lens proteins during senile nuclear cataract formation. *Biochim Biophys Acta* **1977**, *492* (1), 43-52.
11. Wei, M.; Xing, K. Y.; Fan, Y. C.; Libondi, T.; Lou, M. F., Loss of thiol repair systems in human cataractous lenses. *Invest Ophthalmol Vis Sci* **2014**, *56* (1), 598-605.
12. Gutteridge, J. M. C.; Halliwell, B., *Free Radicals in Biology and Medicine*. 5th ed.; Oxford University Press: New York, 2015.
13. Halliwell, B.; Gutteridge, J. M. C., *Free Radicals in Biology and Medicine*. 2015.

14. Mucke, H. A.; Mucke, P.; Mucke, E., Pharmacological therapies for cataract and refractive errors: landscaping niches of ocular drug patenting. *Pharm Pat Anal* **2012**, *1* (2), 165-75.
15. Thiagarajan, R.; Manikandan, R., Antioxidants and cataract. *Free Radic Res* **2013**, *47* (5), 337-45.
16. Peng, Y.-S.; Zhang, J.; Zhao, W.-J.; Ren, B.-C., Inhibitory effect of tiopronin on hydrogen dioxide induced cataract in rabbit. *Yanke Xinjinzhan* **2009**, *29* (2).
17. Kobayashi, S.; Kasuya, M.; Ishii, Y.; Takehana, M.; Sakai, K.; Suzuki, N.; Itoi, M., Effects of 2-mercaptpropionylglycine on the development of X-ray-induced cataract in rats. *Curr Eye Res* **1992**, *11* (11), 1099-103.
18. Jiang, T.-Y.; Sun, C.-S.; Shen, X.; Wang, T.-Y.; Wang, S.-L., Development of a poloxamer analogs/bioadhesive polymers-based in situ gelling ophthalmic delivery system for tiopronin. *J Appl Polym Sci* **2009**, *114* (2), 775-783.
19. Nishigori, H.; Hayashi, R.; Lee, J. W.; Iwatsuru, M., Effect of MPG on glucocorticoid-induced cataract formation in developing chick embryo. *Invest Ophthalmol Vis Sci* **1984**, *25* (9), 1051-5.
20. Kuck, J. F., Jr.; Kuck, K. D., The Emory mouse cataract: the effects on cataractogenesis of alpha-tocopherol, penicillamine, triethylenetetramine, and mercaptpropionylglycine. *J Ocul Pharmacol* **1988**, *4* (3), 243-51.
21. Ichikawa, H.; Imaizumi, K.; Tazawa, Y.; Obara, Y.; Ishikawa, Y.; Tobar, I.; Tanabe, Y., Effect of tiopronin on senile cataracts. A double-blind clinical study. *Ophthalmologica* **1980**, *180* (5), 293-8.
22. Jaffe, I. A., Adverse effects profile of sulfhydryl compounds in man. *Am J Med* **1986**, *80* (3), 471-6.
23. Carlsson, M. S.; Denneberg, T.; Emanuelsson, B. M.; Kagedal, B.; Lindgren, S., Pharmacokinetics of oral tiopronin. *Eur J Clin Pharmacol* **1993**, *45* (1), 79-84.
24. Järvinen, K.; Järvinen, T.; Urtti, A., Ocular absorption following topical delivery. *Adv Drug Deliv Rev* **1995**, *16* (1), 3-19.
25. Abdelkader, H.; Alany, R. G.; Pierscionek, B., Age-related cataract and drug therapy: opportunities and challenges for topical antioxidant delivery to the lens. *J Pharm Pharmacol* **2015**, *67* (4), 537-50.
26. Al-Kinani, A. A.; Zidan, G.; Elsaid, N.; Seyfoddin, A.; Alani, A. W. G.; Alany, R. G., Ophthalmic gels: Past, present and future. *Adv Drug Deliv Rev* **2017**.

27. Kanjickal, D.; Lopina, S.; Evancho-Chapman, M. M.; Schmidt, S.; Donovan, D., Improving delivery of hydrophobic drugs from hydrogels through cyclodextrins. *J Biomed Mater Res A* **2005**, *74* (3), 454-60.
28. Kanjickal, D.; Lopina, S.; Evancho-Chapman, M. M.; Schmidt, S.; Donovan, D., Effects of sterilization on poly(ethylene glycol) hydrogels. *J Biomed Mater Res A* **2008**, *87* (3), 608-17.
29. Galante, R.; Pinto, T. J. A.; Colaco, R.; Serro, A. P., Sterilization of hydrogels for biomedical applications: A review. *J Biomed Mater Res B Appl Biomater* **2017**.
30. Karajanagi, S. S.; Yoganathan, R.; Mammucari, R.; Park, H.; Cox, J.; Zeitels, S. M.; Langer, R.; Foster, N. R., Application of a dense gas technique for sterilizing soft biomaterials. *Biotechnol Bioeng* **2011**, *108* (7), 1716-1725.
31. Schrand, A. M.; Johnson, J.; Dai, L.; Hussain, S. M.; Schlager, J. J.; Zhu, L.; Hong, Y.; Ōsawa, E., Cytotoxicity and Genotoxicity of Carbon Nanomaterials. In *Safety of Nanoparticles*, Webster, T. J., Ed. Springer-Verlag: New York, 2009; pp 159-187.
32. Schrand, A. M.; Hens, S. A. C.; Shenderova, O. A., Nanodiamond Particles: Properties and Perspectives for Bioapplications. *Crit Rev Solid State Mater Sci* **2009**, *34* (1-2), 18-74.
33. Mochalin, V. N.; Gogotsi, Y., Nanodiamond-polymer composites. *Diam Relat Mater* **2015**, *58*, 161-171.
34. Mochalin, V. N.; Shenderova, O.; Ho, D.; Gogotsi, Y., The properties and applications of nanodiamonds. *Nat Nanotechnol* **2011**, *7* (1), 11-23.
35. Mochalin, V. N.; Pentecost, A.; Li, X. M.; Neitzel, I.; Nelson, M.; Wei, C.; He, T.; Guo, F.; Gogotsi, Y., Adsorption of drugs on nanodiamond: toward development of a drug delivery platform. *Mol Pharm* **2013**, *10* (10), 3728-35.
36. Giammarco, J.; Mochalin, V. N.; Haeckel, J.; Gogotsi, Y., The adsorption of tetracycline and vancomycin onto nanodiamond with controlled release. *J Colloid Interface Sci* **2016**, *468*, 253-261.
37. Ho, D., Nanodiamond-based chemotherapy and imaging. *Cancer Treat Res* **2015**, *166*, 85-102.

38. Xi, G.; Robinson, E.; Mania-Farnell, B.; Vanin, E. F.; Shim, K. W.; Takao, T.; Allender, E. V.; Mayanil, C. S.; Soares, M. B.; Ho, D.; Tomita, T., Convection-enhanced delivery of nanodiamond drug delivery platforms for intracranial tumor treatment. *Nanomedicine* **2014**, *10* (2), 381-91.
39. Roy, U.; Drozd, V.; Durygin, A.; Rodriguez, J.; Barber, P.; Atluri, V.; Liu, X.; Voss, T. G.; Saxena, S.; Nair, M., Characterization of Nanodiamond-based anti-HIV drug Delivery to the Brain. *Sci Rep* **2018**, *8* (1), 1603.
40. Chow, E. K.; Zhang, X. Q.; Chen, M.; Lam, R.; Robinson, E.; Huang, H.; Schaffer, D.; Osawa, E.; Goga, A.; Ho, D., Nanodiamond therapeutic delivery agents mediate enhanced chemoresistant tumor treatment. *Sci Transl Med* **2011**, *3* (73), 73ra21.
41. Lim, D. G.; Kim, K. H.; Kang, E.; Lim, S. H.; Ricci, J.; Sung, S. K.; Kwon, M. T.; Jeong, S. H., Comprehensive evaluation of carboxylated nanodiamond as a topical drug delivery system. *Int J Nanomedicine* **2016**, *11*, 2381-2395.
42. Adach, K.; Fijalkowski, M.; Skolimowski, J., Antioxidant Effect of Hydroxylated Diamond Nanoparticles Measured in Soybean Oil. *Fuller Nanotub Car N* **2015**, *23* (12), 1024-1032.

VITA

Justin Edward Beltz completed a Bachelor of Science in chemistry with an emphasis in biochemistry at Missouri University of Science and Technology in Rolla, Missouri in December 2014. As an undergraduate student, he conducted research on the role of oxidative stress in Alzheimer's disease and Diabetes in Dr. Nuran Ercal's research group. In 2015, he entered the Doctor of Philosophy program in the chemistry department at Missouri University of Science and Technology. During his residency as a graduate student in the chemistry department, Justin mentored twelve undergraduate students through the completion of individual undergraduate research projects. Justin was awarded the Outstanding Graduate Teaching award for the Physical Chemistry Laboratory and General Biochemistry Laboratory courses for the 2015-2016 academic year. He was also awarded First Place at the Graduate Research Showcase Poster Competition hosted by the Council of Graduate Students in 2016. In 2019, Justin was awarded First Place at the Three-Minute Thesis Competition held at Missouri University of Science and Technology. His research interests included analytical method development, drug delivery, oxidative stress, additive manufacturing, and development of open-source laboratory equipment. He received his Doctor of Philosophy in chemistry from Missouri University of Science and Technology in December 2020.